SILICON MATERIALS TASK OF THE LOW COST
SOLAR ARRAY PROJECT (PHASE III)

DRD No. SE-7
DRL No. 58

Dist. Category UC-63
DOE/JPL-954331-79/2

Effect of Impurities and Processing on Silicon Solar Cells

Fourteenth Quarterly Report

April, 1979

January 1979-March 1979

R. H. Hopkins, J. R. Davis, P. D. Blais,
A. Rohatgi, R. B. Campbell, P. Rai-Choudhury and R. E. Stapleton
Westinghouse Research & Development Center
and
H. C. Mollenkopf and J. R. McCormick
Dow Corning Corporation

Contract No. 954331

The JPL Low Cost Silicon Solar Array Project is sponsored by the U. S. Dept. of Energy and forms part of the Solar Photovoltaic Conversion Program to initiate a major effort toward the development of low-cost solar arrays. This work was performed for the Jet Propulsion Laboratory, California Institute of Technology by agreement between NASA and DOE.

Westinghouse R&D Center
1310 Beulah Road
Pittsburgh, Pennsylvania 15235

SILICON MATERIALS TASK OF THE LOW COST
SOLAR ARRAY PROJECT (PHASE III)

Effect of Impurities and Processing on Silicon Solar Cells

Fourteenth Quarterly Report

April, 1979

January 1979-March 1979

R. H. Hopkins, J. R. Davis, P. D. Blais.
A. Rohatgi, R. B. Campbell, P. Rai-Choudhury and R. E. Stapleton
Westinghouse Research & Development Center
and
H. C. Mollenkopf and J. R. McCormick
Dow Corning Corporation

Contract No. 954331

The JPL Low Cost Silicon Solar Array Project is sponsored by the U. S. Dept. of Energy and forms part of the Solar Photovoltaic Conversion Program to initiate a major effort toward the development of low-cost solar arrays. This work was performed for the Jet Propulsion Laboratory, California Institute of Technology by agreement between NASA and DOE.

Westinghouse R&D Center
1310 Beulah Road
Pittsburgh, Pennsylvania 15235

TECHNICAL CONTENT STATEMENT

This report was prepared as an account of work sponsored by the United States Government. Neither the United States nor the United States Department of Energy, nor any of their employees, nor any of their contractors, sub-contractors, or their employees, makes any warranties, express or implied, or assumes any legal liability or responsibility for the accuracy, completeness or usefulness of any information, apparatus, product or process disclosed, or represents that its use would not infringe privately owned rights.

NEW TECHNOLOGY

No new technology is reportable for the period covered by this report.

TABLE OF CONTENTS

TABLE OF CONTENTS (Cont.)

LIST OF ILLUSTRATIONS

LIST OF ILLUSTRATIONS (Cont.)

LIST OF TABLES

1. SUMMARY

This is the 14th quarterly report of a DOE/JPL sponsored program designed to assess the effects of impurities, thermochemical processes and any impurity process interactions on the performance of terrestrial silicon solar cells. The data developed form a basis for cost benefit analyses by the producers and users of Solar Grade Silicon.

The Phase III effort encompases (1) potential interactions between impurities and thermochemical processing of silicon, (2) impurity-cell performance relationships in n-base silicon, (3) effect of contaminants introduced during silicon production, refining or crystal growth on cell performance, (4) effects of non-uniform impurity distributions in large area silicon wafers, and (5) a preliminary study of the permanence of impurity effects in silicon solar cells.

Phosphorus oxychloride gettering of low resistivity ingots (0.2 Ω cm) infused with Ti produced cell efficiency improvements virtually identical to those observed during gettering of 4 Ω cm material bearing Ti. For example, the uncoated cell efficiency rose to 6.2% (after 5 hours treatment at 1100°C) compared to an untreated value of 4.4%. A low resistivity Mo-doped ingot exhibited no improvement in cell efficiency after a similar gettering cycle; this was consistent with previous data for 4 Ω cm Mo-doped silicon.

Deep level transient spectroscopy (DLTS) and detailed I-V measurements made on gettered Ti-doped solar cells indicate that as cell performance improves, bulk lifetime increases and the density of Ti recombination centers (E_V + 0.3 eV level) diminishes. Thus gettering deactivates the recombination centers rather than changing the level of the recombination center. The Ti trap density fell by about a factor of four after gettering for 5 hours at 1100°C.

Studies of potential impurity anisotropy in 3 inch Mo and Ti-doped wafers were extended to provide detailed edge to center and seed to tang maps of cell performance. No systematic or preferential impurity distribution was noted save for a slight seed to tang buildup due to impurity segregation during crystal growth. Performance variation across or along the ingots was within $\pm$ 10% of the average ingot cell efficiency. This was consistent with the map of ingot bulk lifetime which indicated the maximum variation of impurity content to be less than a factor of two in both types of ingots.

Initial studies of impurity aging effects on solar cells have been completed for temperatures up to 800°C and for times as long as 100 hours. No cell performance degradation due to aging effects in Mo or Ti-doped cells was noted even at the longest times and temperatures. However, cell efficiency reduction did occur in contacted cells after 10 hours at 500°C due to interdiffusion of the contact metals and silicon base material.

2. INTRODUCTION

This is the 14th quarterly report describing activities conducted under JPL Contract 954331. Phase III of this program is entitled "An Investigation of the Effects of Impurities and Processing on Silicon Solar Cells."

The objective of this program is to determine how various processes, impurities, and impurity-process interactions affect the properties of silicon and the performance of terrestrial solar cells made from silicon. The development of this data base permits the definition of the tolerable impurity levels in a low-cost Solar Grade Silicon. The data further provide the silicon manufacturer with a means to select materials of construction which minimize product contamination and permit the cost-effective selection of chemical processes for silicon purification. For the silicon ingot, sheet, or ribbon manufacturer, the data suggest what silicon feedstock purity must be selected to produce wafers suitable for cell production and what furnace materials minimize wafer contamination: the cell manufacturer may use the data to define an acceptable wafer purity for cell processing or to identify processes which minimize impurity impact on efficiency. In short, the data provide a basis for cost-benefit analysis to the producers and users of Solar Grade Silicon.

The Phase III effort encompasses five major topics, several of which represent new directions for our work: (1) examination of the interaction of impurities with processing treatments, (2) generation of a data base and modeling of impurity effects in n-base solar cells, (3) extension of previous p-base studies to include impurities likely to be introduced during silicon production, refining or crystal growth, (4) a consideration of the potential impact of anisotropic (nonuniform) impurity distribution in large Czochralski and ribbon solar cells and,

(5) a preliminary investigation of the permanence of impurity effects in silicon solar cells.

During this quarter we have (1) examined in detail the mechanisms responsible for impurity deactivation during high temperature gettering treatments, (2) evaluated the seed to tang and center to edge variation in Czechralski ingot properties for commercial-size ingots doped with Ti and Mn, and (3) assessed aging effects in solar cells doped with Ti or Mo. We have also continued our analyses of impurity effects on crystal structure breakdown, and the monitoring of ingot lifetimes by photoconductive decay lifetime measurement before and after processing. The highlights of this work are described below.

3. TECHNICAL RESULTS

3.1 Growth and Evaluation of Silicon Ingots

Major objectives of this activity have been to provide ingots purposely contaminated with controlled additions of metal impurities for subsequent electrical and solar cell evaluation and also to assess the effects of impurities on ingot microstructure. During this quarter, besides the preparation and analysis of Czochralski ingots, we have also estimated the segregation coefficient of Co in silicon and measured the critical melt impurity concentrations of Co, W, and Fe at which loss of single crystal structure occurs.

3.1.1 Ingot Preparation

Seventeen ingots (W155 to W171, inclusive) were grown by Czochralski pulling, using the same techniques and conditions described in previous reports.[1,2] Five of these were second and third generation ingots doped with phosphorus and one or more metal impurities to complete the data base on impurity effects in n-base solar cells. The remainder of the crystals included ingots designated for synergy studies, studies of materials of construction, and compensation experiments.

All ingots, target impurity concentrations, impurity concentrations based on melt analysis and impurity concentrations measured by spark source mass spectrometry[2,3] are listed in Appendix 1. Table 1 shows our best estimates of the impurity concentrations for the ingots grown to date. These latter values are used in all modeling calculations and experimental correlations.

Table 1. Best Estimate of Impurity Concentrations

Ingot Identification	Best Estimate of Impurity Concentration ($X10^{15}$ atoms/cm^3)
W-129-00-000 (7.6 cm)	NA
W-130-00-000 (7.6 cm)	NA
W-131-Mn-008 (7.6 cm)	0.55
W-132-Ta-003	0.0002
W-133-00-000	NA
W-134-Ti-009	0.05
W-135-Fe-005	1.0
W-136-Fe-006	0.3
W-137-Ti-010	0.21
W-138-Mo-005	0.001
W-139-Mo-006	0.0042
W-140-Ti-001 (7.6 cm)	0.18
W-141-Mo/Cu-001	0.004/4.00
W*-142-00-000	NA
W*-143-Ti-002	0.20
W-144-Mo-001	0.004
W-145-W-001	<0.15
W-146-Co-001	<1.7
W-147-N/Ni-002	0.40
W-148-N/Mn-002	0.60
W-149-N/Fe-003	0.60
W-150-N/V-003	0.03
W**-151-00-000	NA
W**-152-Ti-001	0.21
W-153-N/Ti-003	0.013

Table 1. Best Estimate of Impurity Concentrations Cont.

Ingot Identification	Best Estimate of Impurity Concentrations (X 10^{15} atoms/cm^3)
W-154-N/Cr-003	0.50
W-155-N/Mo-001	0.001
W-156-N/Mo-002	0.004
W-157-N/Ti/V-001	0.10/0.10
W-158-N/Ti/V/Cr-001	0.05/0.05/0.60
W-159-N/Cr/Mn/Ti/V-001	0.30/0.30/0.03/0.02
W*-160-Ti-001	0.20
W**-161-Ti-002	0.02
W-162-Ni/Ti-001	1.0/0.20
W-163-Ni/V-001	1.0/0.27
W-164-Ni/Mo-001	1.0/0.004
W-165-Co-002	0.11
W-166-Fe-007	0.9
W-167-Nb-001	Processing
W*-168-Ph-002	110+
W*-169-Ph-004	136+
W-170-Ph-005	Processing
W-171-W-002	Processing

* Asterisk indicates low resistivity p-type ingot ($\leq$ 1 Ω-cm)

** 30 Ω-cm p-type ingot

\+ Value based on resistivity measurement

3.1.2 Ingot Evaluation

The resistivity and etch pit density for each ingot (Appendix 2) continue to fall close to the norms established throughout the course of Phases I and II of this program. As before, we note that the dislocation densities measured toward the seed end of the ingots are similar to those of the material fabricated into solar cells. Structural breakdown often occurs near the tang end of the heavily-doped ingots.[1]

The carbon and oxygen concentrations of each odd numbered ingot were measured by infrared absorption. The amplitude of the absorption peaks at 606 cm^{-1} and 1107 cm^{-1} is proportional to the carbon and oxygen concentrations, respectively. The constants of proportionality used in these measurements were 2.2 for carbon and 9.6 for oxygen.[2] Typical carbon and oxygen concentrations in Czochralski grown material are in the range of 2.5 to $5x10^{17}$ atoms/cm^3 for carbon and 50 to $150x10^{16}$ atoms/cm^3 for oxygen. We found no significant deviations from these values in the ingots produced this quarter (see for example, Appendix 3).

3.1.3 Segregation Coefficients of Co and W

In a previous report[4] we described the results of ingot and melt analyses which placed an upper limit on the segregation coefficient of cobalt in silicon at $1.1x10^{-5}$ and of tungsten at $1.6x10^{-6}$. The limits were based on our inability to detect Co or W by spark source mass spectroscopy in the most heavily-doped ingots so far produced.

The detection of cobalt in a silicon spectrum by mass spectroscopy is hindered by the intense silicon background produced by the lines of Si^+ at m/e. = 28 and 29.[4] By cutting the photoplate at the position of the Si 28 line prior to exposure it was possible to eliminate enough of the Si background to detect the Co line at m/e = 29 1/2. This analytical result set the Co concentrations of ingot W146 at $5.5x10^{14}$ atoms cm^{-3}. Dividing this value by the measured melt concentration $1.5x10^{20}$ atoms cm^{-3} yields a Co segregation coefficient for Czochralski pulling of $3.7x10^{-6}$.

Additional mass spectrographic evaluation of W-doped ingot W145 did not provide as salutary a result as that for Co. Even prolonged exposure of samples from the tang end of the ingot failed to reveal lines attributable to W. We, therefore, presently place the best estimate of the impurity concentration for ingot W145 at about $1x10^{12}$ cm^{-3} based on a segregation coefficient of $1x10^{-8}$ estimated for tungsten.[5]

Additional analyses of ingots bearing Co and W (as well as Mo, Ta, Fe, Ti, and Ni) will be carried out by sensitive neutron activation analysis.[1] This data should provide a firmer foundation for the segregation coefficient values.

3.1.4 Structural Breakdown Via Constitutional Supercooling

The breakdown of a planar single crystal-liquid interface to a cellular polycrystalline morphology is well documented in ceramics, metals and semiconductors. For Czochralski growth of silicon we showed that the critical liquid impurity content C_ℓ^* for which breakdown occurs is given by an equation of the form[2]

$$C_\ell^* = -\frac{D}{m}\left[\frac{A}{r^{1/2}V} - B\right] \qquad (1)$$

where D is the liquid diffusion coefficient of an impurity, m the liquidus slope of the phase diagram, r the crystal radium (cm) and V is the growth velocity (cm/sec). The expected variation in critical impurity concentration with growth speed is graphed in Figure 1 for different crystal radii. Superposed on the curves are data for our typical 3.2 to 3.5 cm diameter ingots doped with Co, W and Fe, respectively. The data were obtained from observations of the location in an ingot at which structural breakdown occurred, the measured volume fraction of the melt frozen and the measured melt impurity concentration. The measured and calculated breakdown concentrations are in good agreement for these impurities. The data are also consistent with previous results for other impurities:[1,2] breakdown at 7-8 cm/hr growth rates occurs at impurity concentrations near 10^{20} cm^{-3} for these 1.6 to 1.7 cm radii ingots.

Curve 715943-A

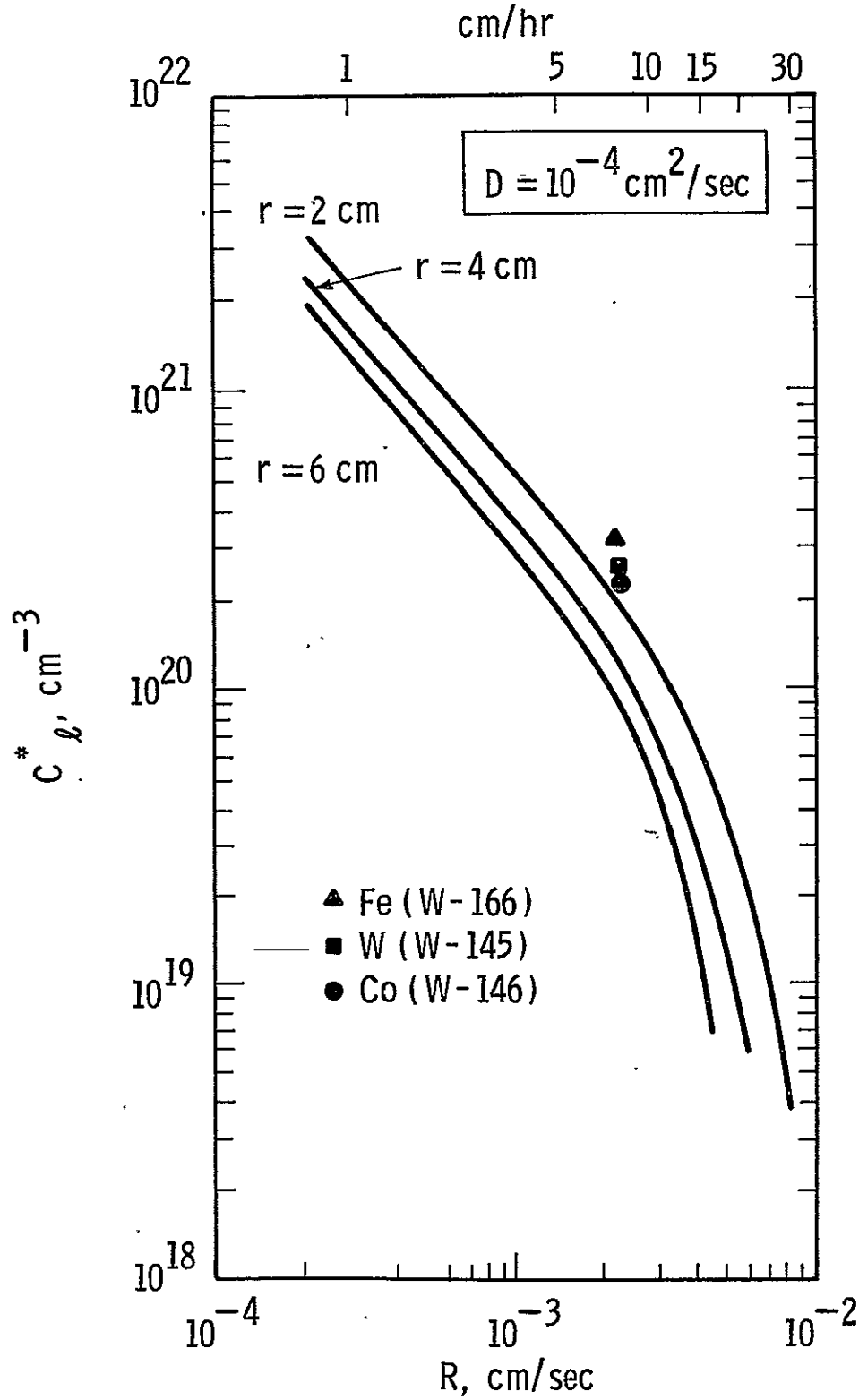

Figure 1 Predicted variation of critical liquid impurity concentration for crystal breakdown with crystal growth velocity during Czochralski pulling of silicon. Data points represent impurity concentrations at which breakdown actually took place (curves assume heat loss to 0°K environment, see Reference 2)

3.2 Processing Studies

3.2.1 Effect of Thermochemical Processing on the Performance of Impurity-Contaminated Solar Cells

The treatment of silicon wafers at elevated temperatures in the presence of a chemical species such as $POCl_3$ or HCl provides a mechanism to neutralize, or getter, contaminants subsequent to the crystal growth operation. In principle, the method may be used to improve the performance of solar cells fabricated on impurity-bearing material. We are carrying out a series of experiments to identify the magnitude and temperature-time sensitivity of gettering effects for impurities like Ti which are known to degrade solar cell efficiency.[1,2]

The experimental approach was to subject impurity-doped and uncontaminated baseline wafers to various thermal treatments in the presence of $POCl_3$ or HCl after which the gettered surface was etched off. The gettered wafers, fabricated into solar cells via our standard process, were then tested and the results compared to the performance of the baseline devices.

The first results of this study, $POCl_3$ gettering of 4 Ωcm Fe, Ti and Mo-doped ingots, were reported in the last quarterly report.[4] The key data are reproduced in Figure 2 to facilitate some of the discussion which follows below. Briefly, the conclusions derived from that work were that for gettering temperatures in the range 950 to 1100°C and time periods up to five hours:

1. The cell performance of the Mo-doped ingots was improved little, if at all, by $POCl_3$ gettering.
2. The cell efficiencies of the two Ti-doped ingots improved considerably but very extended times or high temperatures would be required to promote recovery to the baseline efficiency values.
3. The efficiency of the Fe-doped ingot recovered to that of the baseline value.

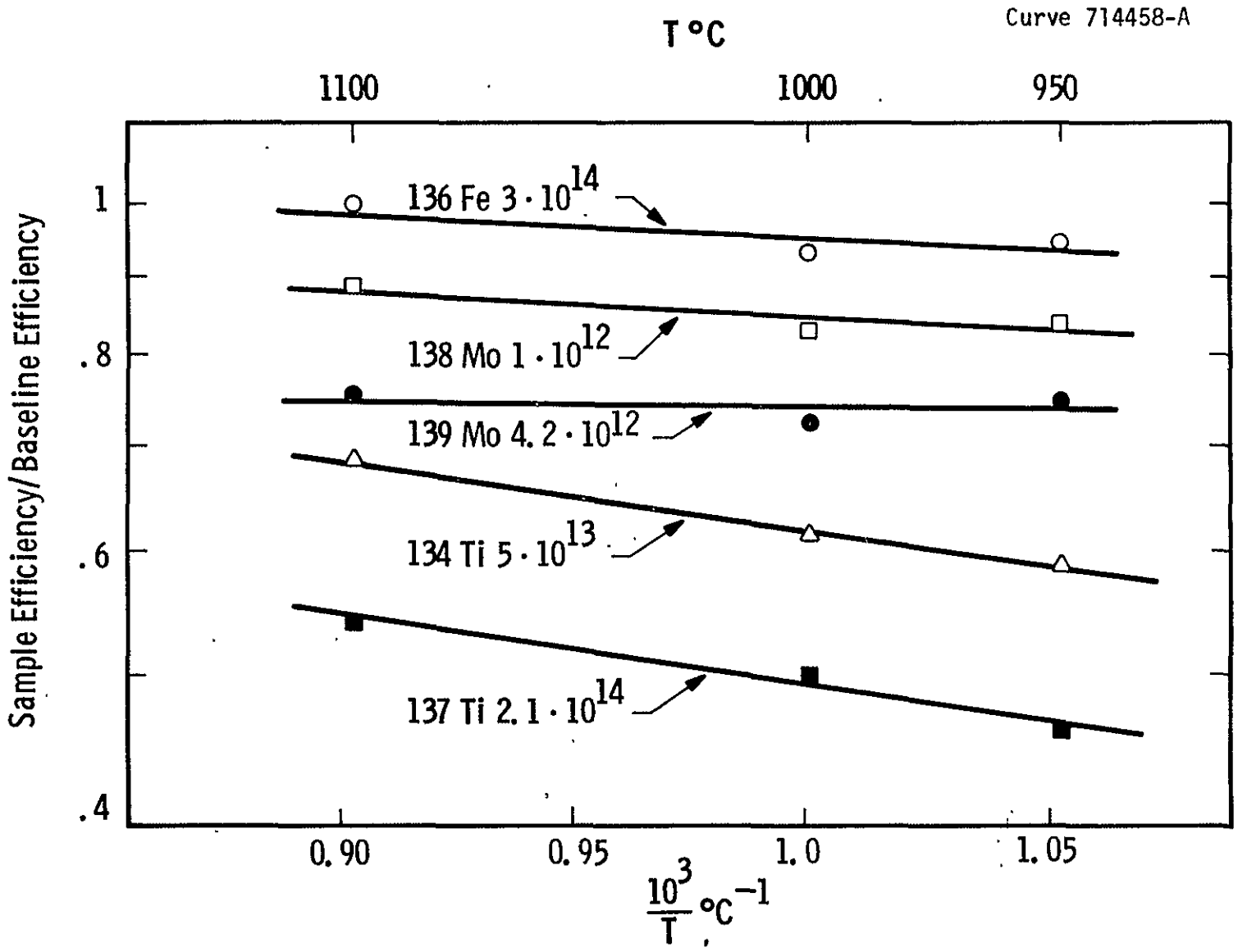

Figure 2 Normalized efficiency for isochronal $POCl_3$ gettering (1 hours)

4. The baseline ingot efficiency degraded somewhat at the higher gettering temperature; if this phenomenon were intrinsic it could place an upper limit on the effectiveness of $POCl_3$ treatments to improve cell efficiency.

The $POCl_3$ gettering experiments have been extended to evaluate the impact of base resistivity as well as impurity content on gettering response. Wafers from two low resistivity (0.2 Ωcm) ingots, W*143Ti002 ($2x10^{14}$ cm^{-3} Ti) and W*144Mo001 ($4x10^{12}$ cm^{-3} Mo), were processed along with low resistivity baseline ingot W*142-00-000 at the following times and temperatures:

1 hr at 950°C
1 hr at 1000°C
1 hr at 1100°C
2 hrs at 1100°C
3 hrs at 1100°C
4 hrs at 1100°C

The cell performance data for each condition as well as for the untreated material are listed in Tables 2 and 3. In the tables, the designation B refers to the baseline ingots, I to the impurity-doped ingots and I/B to the ratio of the performance values for the impurity-doped and the baseline materials, respectively.

The data for the low resistivity Ti ingot (W*143), Table 2, is in general agreement with the trends established earlier for the 4 Ωcm ingot W137 which contains the same nominal Ti content. After 5 hours treatment at 1100°C, the uncoated efficiency of ingot W*143 increased to 6.43% from the untreated value of 4.42%.

This trend is illustrated graphically in Figure 3 where the relative efficiencies (η/η baseline) are plotted for ingots W*143 and W137 as a function of treatment temperature for a one hour gettering cycle. The relative efficiency of the low resistivity devices improves to 0.63 from the untreated value of 0.46. The slope of the lines for Ti gettering in the low and high resistivity material is approximately

TABLE 2 - $POCl_3$ GETTERING - LOW RESISTIVITY Ti INGOT

Ingot W143Ti002 ($2x10^{14}cm^{-3}$ Ti; 0.2 Ωcm)

Baseline Ingot W14200 000

TREATMENT		I_{SC}(mA)	V_{OC}(V)	FF	EFF*(%)	τ_{OCD} (μsec)
NONE	B	20.40	.598	.752	9.69	1.8
	I	10.90	.525	.728	4.42	1.1
	I/B	.534	.878	.968	.456	.611
1 Hr. @ 950°C	B	20.47	.599	.752	9.76	5.2
	I	11.68	.539	.748	4.99	1.5
	I/B	.571	.900	.995	.511	.288
1 Hr. @ 1000°C	B	20.44	.594	.708	9.09	1.1
	I	11.60	.541	.755	5.01	1.5
	I/B	.567	.910	1.07	.551	1.36
1 Hr. @ 1100°C	B	20.50	.595	.711	9.18	1.2
	I	12.96	.551	.739	5.58	1.3
	I/B	.632	.926	1.04	.608	1.08
2 Hr. @ 1100°C	B	20.57	.596	.774	10.12	1.5
	I	13.04	.549	.739	5.65	1.4
	I/B	.633	.921	.955	.558	.933
3 Hrs. @ 1100°C	B	20.70	.598	.758	9.93	1.6
	I	13.68	.560	.756	6.12	1.0
	I/B	.661	.936	1.00	.616	.62
5 Hrs. @ 1100°C	B	20.37	.602	.766	9.92	1.6
	I	13.90	.554	.756	6.23	1.1
	I/B	.682	.920	.987	.628	.687

*AM1; no AR coating

TABLE 3 - $POCl_3$ GETTERING - LOW RESISTIVITY Mo INGOT

Ingot W144Mo001 (4×10^{12} cm^{-3} Mo; 0.2 Ωcm)

Baseline Ingot W14200 000

TREATMENT		I_{SC} (mA)	V_{OC} (V)	FF	EFF* (%)	τ_{OCD} (μsec)
NONE	B	20.40	.598	.752	9.69	1.8
	I	17.46	.539	.642	6.46	.71
	I/B	.856	.901	.854	.667	.39
1 Hr. @ 950°C	B	20.57	.585	.735	9.47	1.2
	I	17.20	.569	.709	7.34	1.0
	I/B	.836	.973	.965	.775	.83
1 Hr. @ 1000°C	B	20.10	.597	.788	10.00	1.69
	I	16.45	.540	.622	5.80	.4
	I/B	.818	.905	.789	.580	.24
1 Hr. @ 1100°C	B	20.30	.601	.784	10.11	1.56
	I	17.00	.550	.595	6.00	.7
	I/B	.837	.915	.759	.593	.45
2 Hrs. @ 1100°C	B	20.57	.600	.775	10.11	2.6
	I	17.50	.558	.556	5.74	.5
	I/B	.851	.930	.717	.571	.19
3 Hrs. @ 1100°C	B	20.40	.599	.769	9.94	1.6
	I	-	-	-	-	-
	I/B	-	-	-	-	-
5 Hrs. @ 1100°C	B	20.40	.600	.769	9.95	1.5
	I	-	-	-	-	-
	I/B	-	-	-	-	-

*AM1; no AR coating

Curve 715942-A

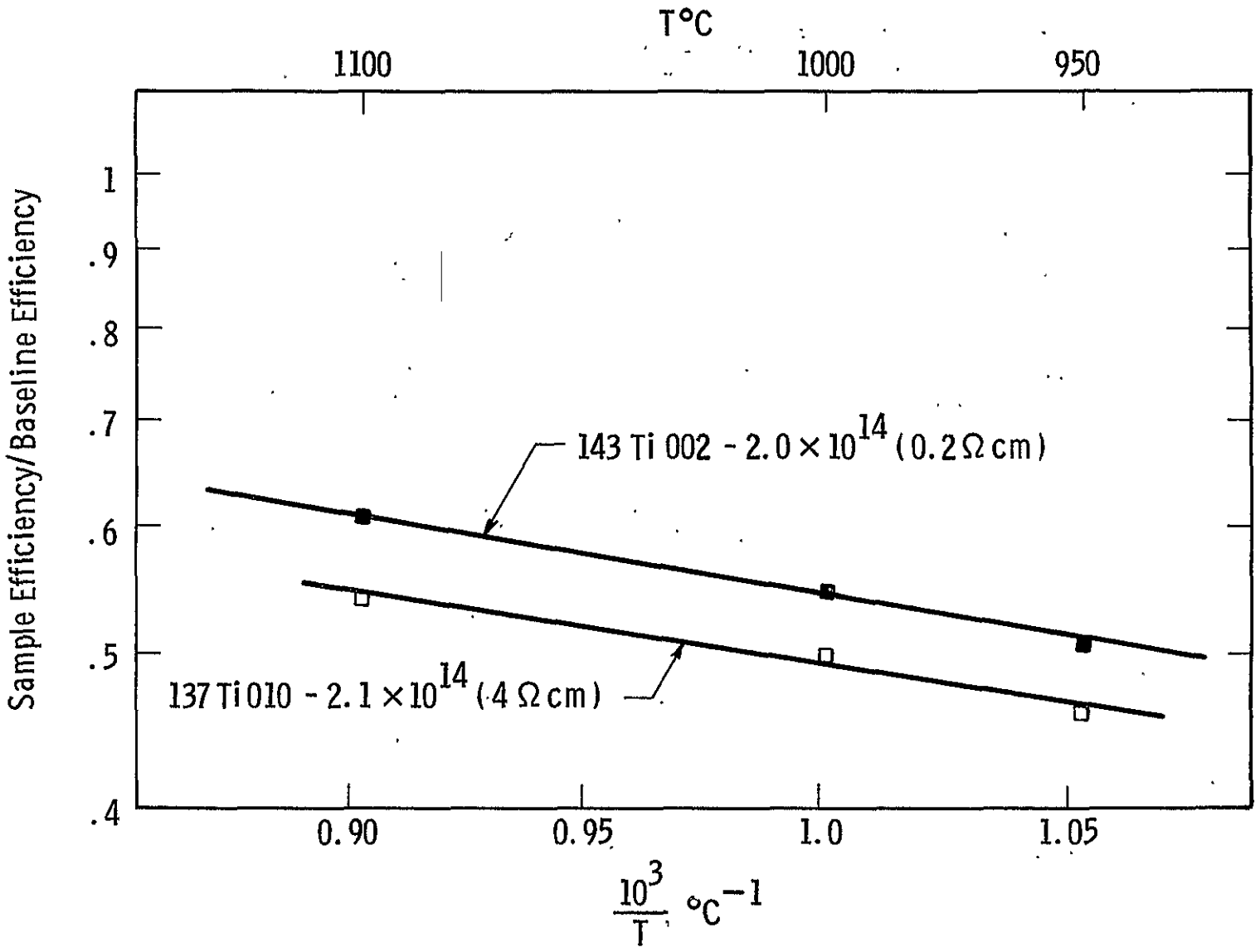

Figure 3 Variation in the normalized efficiency of low and high resistivity Ti-doped ingots with $POCl_3$ gettering (1 hours)

the same, suggesting that the same mechanism of impurity deactivation operates for both ingots over the range of temperatures studied so far. Again the trends depicted in Figure 3 imply that long times and high temperatures would be required to achieve cell efficiencies comparable to the baseline material if ingots initially contain high Ti concentrations.

The cell data for the low resistivity Mo-doped material (ingot W144*), Table 3, also parallel the results obtained earlier for the 4 Ωcm ingot. There is little noticeable improvement in cell efficiency even at the longest treatment time and highest temperature. We noted considerable scatter in the data. Moreover, specimens treated for 3 hr and 5 hr periods at 1100°C exhibited uncoated efficiencies of 1% or below. The latter result may be real or due to processing faults. In either case the small impact of gettering on both the low and high resistivity Mo-doped material at 1100°C suggests that little further benefit will be gained by repeating the runs.

We also note that unlike the first experiments[4] we found no degradation in the baseline properties of the 0.2 Ωcm control ingot (W142*) due to gettering. This aspect of the experiments will be examined in future studies.

Besides $POCl_3$ gettering we have also performed HCl gettering on 4 and 0.2 Ωcm ingots doped with Fe, Ti and Mo. The full spectrum of samples has not yet been completely analyzed. However, the preliminary results indicate that the HCl treatment is somewhat more effective than $POCl_3$ gettering in the 4 Ωcm material. This work will be completed and reported at the end of the next quarter.

3.2.2 Detailed Analysis of the $POCl_3$ Gettering of Ti-Doped Silicon

3.2.2.1 I-V Studies of Gettered Material

The improvement in the cell performance due to $POCl_3$ gettering of Ti in ingot W134 and W137 was described briefly above and is evident from Figure 2. The mechanism by which gettering improves cell efficiency is not so clear from the cell data or the OCD lifetime measurements on the cells.[4]

For example, the OCD lifetimes on the gettered cells were very low (τ_{OCD} < 1 μsec) and the changes in the lifetime for the various gettering conditions fell within the accuracy of the OCD technique. Thus it was not possible to use this method to distinguish how the gettering induced the cell performance improvement. For these reasons, detailed I-V measurements have been made on the gettered cells to track the changes in electrical properties due to thermal treatment. These measurements are complemented by results from deep level transient spectroscopy (DLTS) outlined in the next section.

The transformed I-V curves for the extreme cases of gettering temperature (1 hour - 950 and 1100°C) and gettering time (1100°C - one hour and 5 hours) are shown in Figures 4 and 5 for ingot 137 and Figures 6 and 7 for ingot 134. It is quite clear from these transformed I-V curves that the increase in gettering time and temperature beyond 950°C* increased the bulk lifetime because the upper segment of the transformed curves moved to the right[1] with increased gettering intensity.

From the data in Figures 4-7, we have also deduced the actual lifetime increase due to processing. The short-circuit current of the solar cell is a more accurate indicator of the bulk lifetime than the OCD number because the OCD technique is more sensitive to junction defects surface shunts and other process-related effects. The data in Tables 4 and 5 clearly demonstrate a systematic increase in the short-circuit current as either gettering time or temperature increase. This implies that the bulk lifetime also shifts upward systematically. We have calculated bulk lifetime from the short-circuit current using the impurity model as a basis.[1,2] This is done by employing the model equation (Equation 45 Reference 1, p. 67):

---

* There is little difference in the cell efficiency or I-V curves for the 950°C-1 hr treatment and the standard 850°C-30 min cell diffusion. This suggests that Ti gettering occurs as well at 850°C and/or Ti is a relatively slowly diffusing species

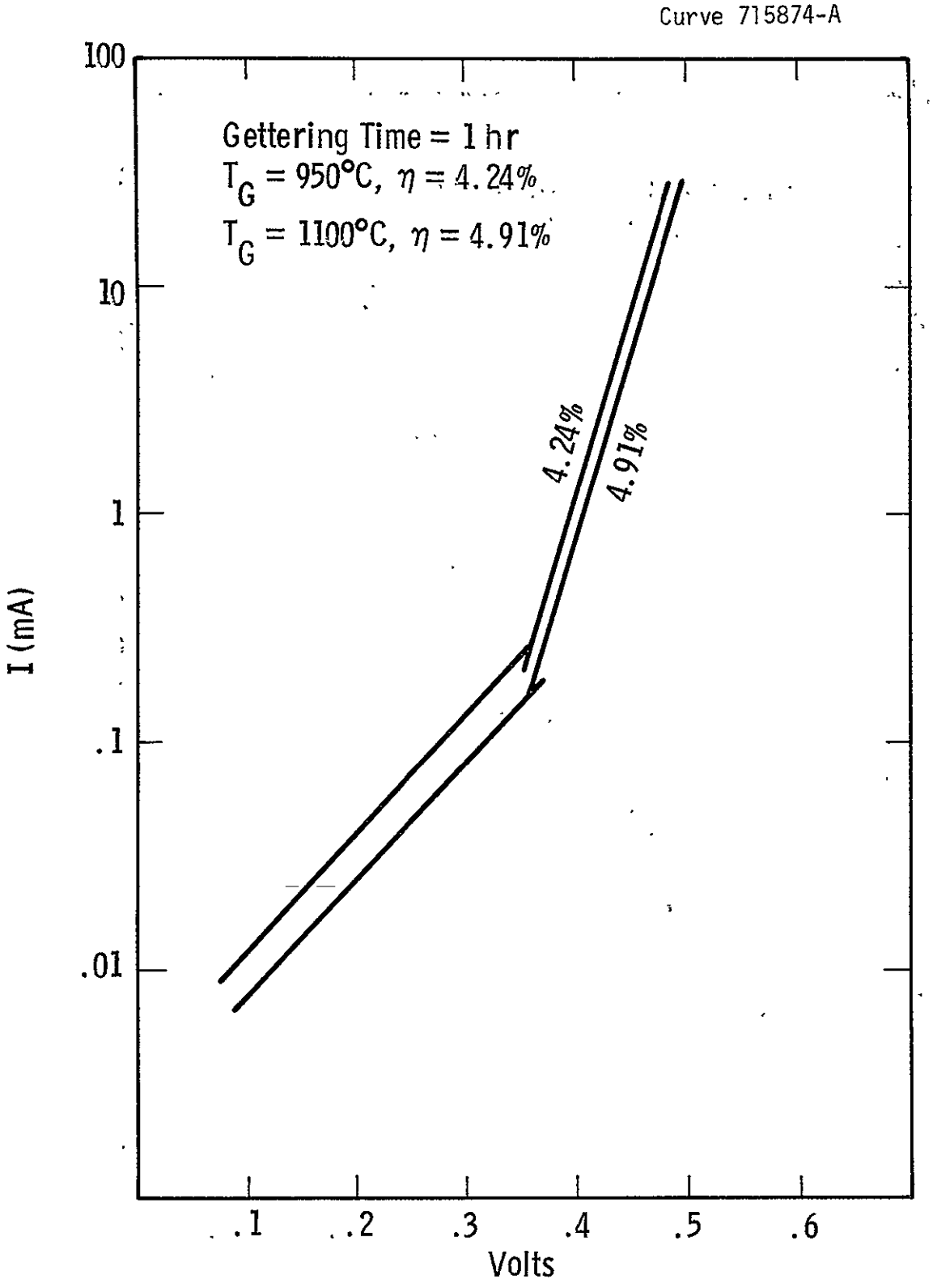

Figure 4 Effect of $POCl_3$ Gettering Temperature on Ingot W137Ti010

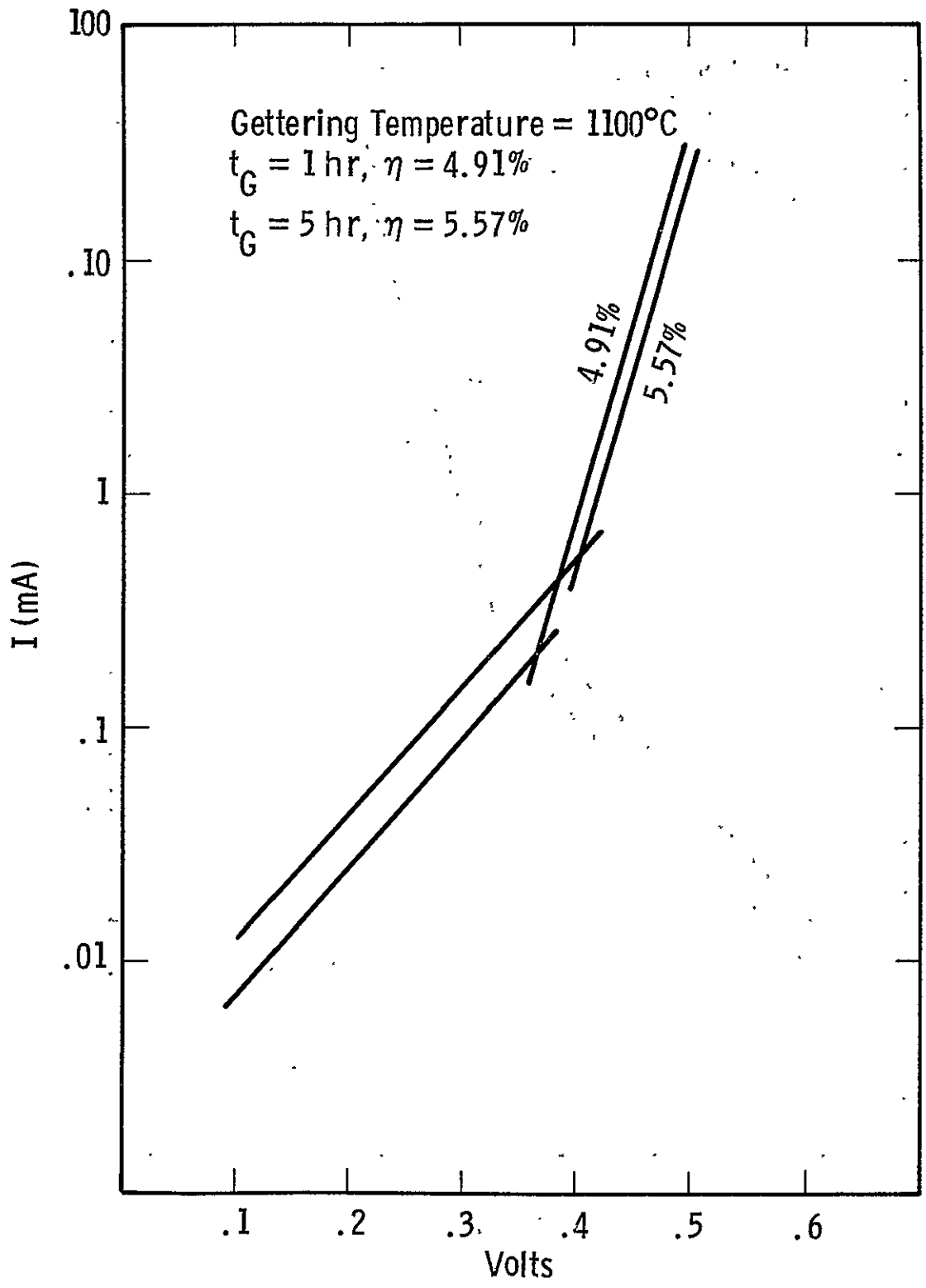

Figure 5 Effect of $POCl_3$ Gettering Time on Ingot W137Ti010

Curve 715873-A

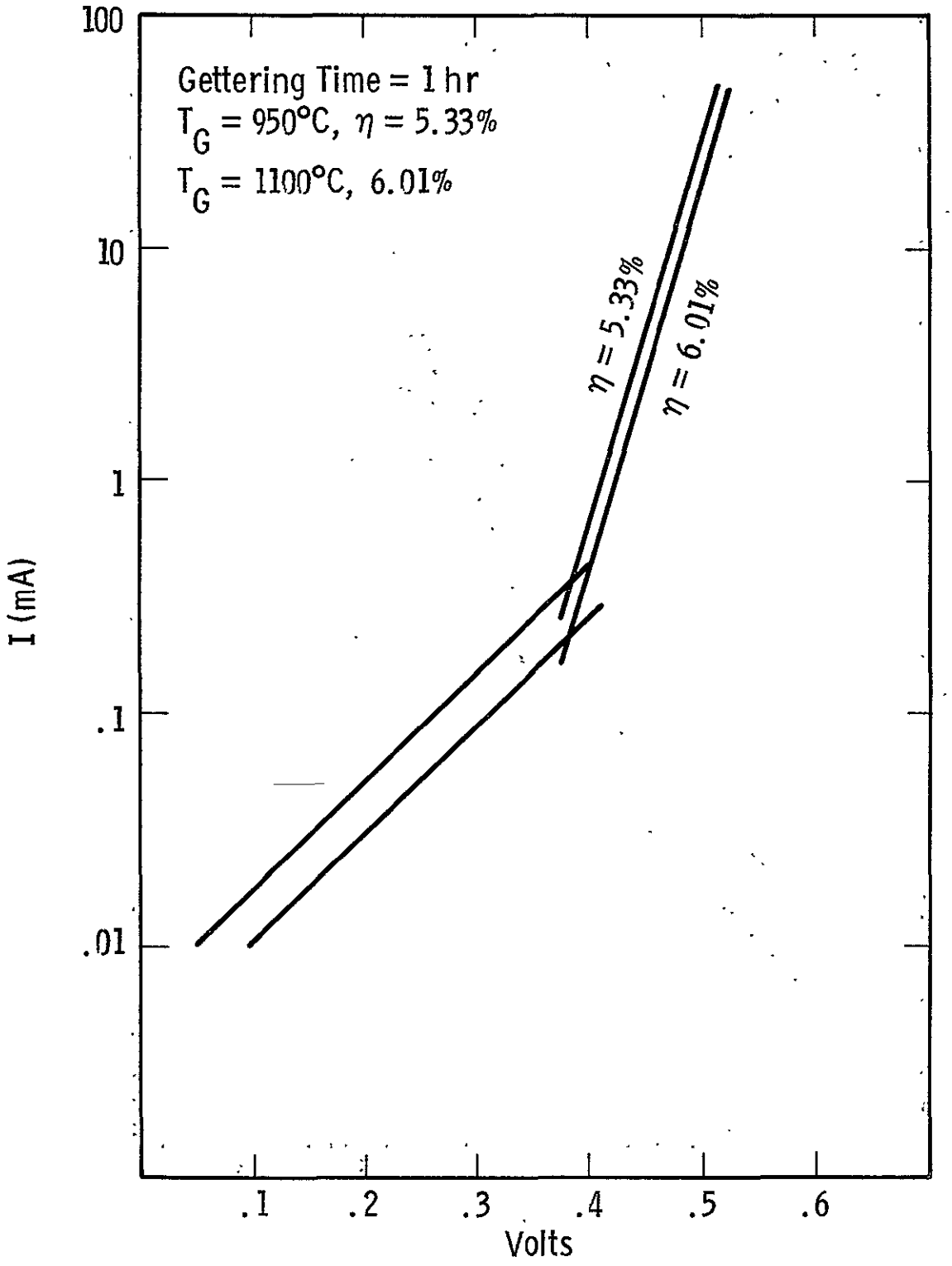

Figure 6 Effect of $POCl_3$ Gettering Temperature on Ingot W134Ti009

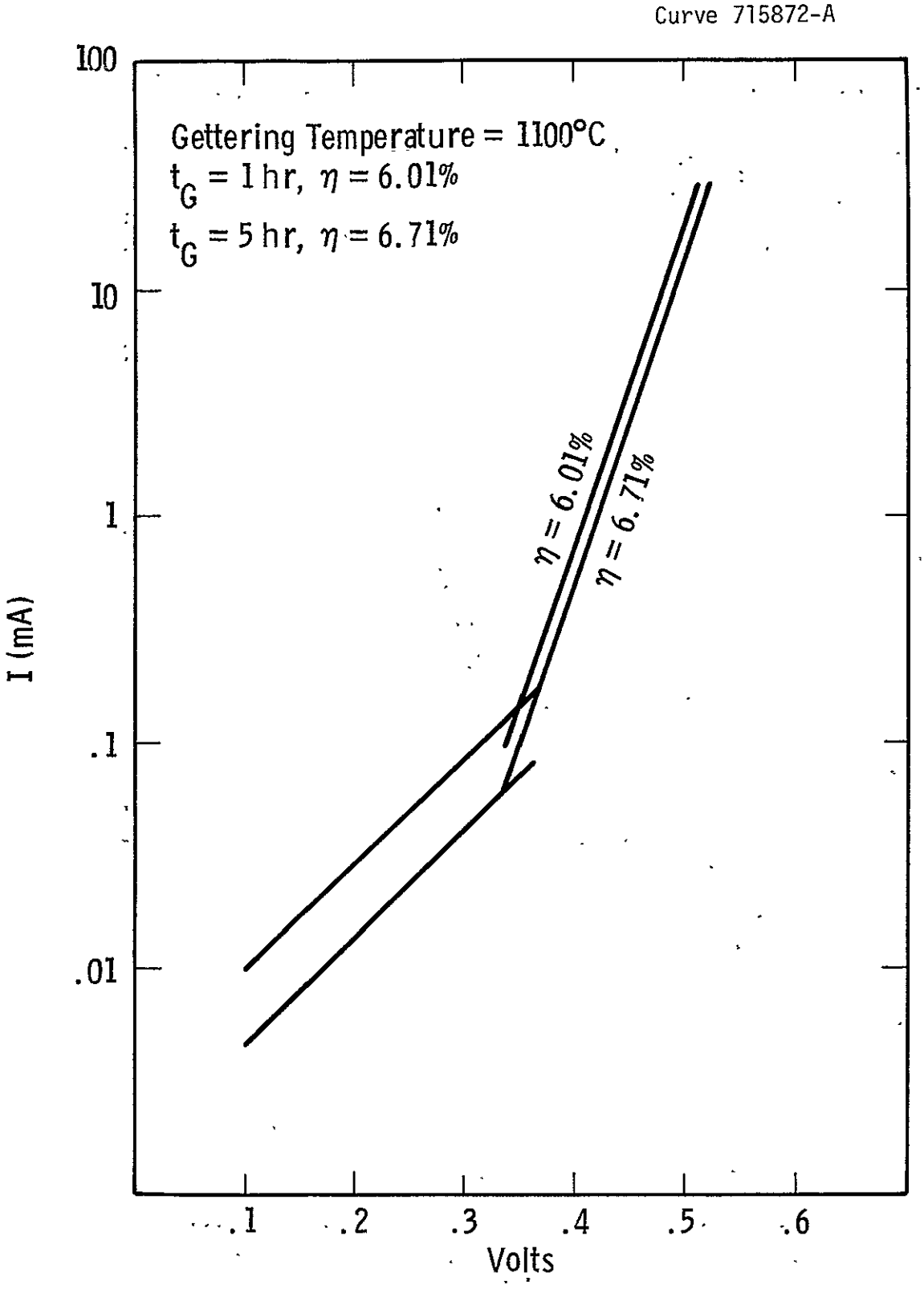

Figure 7 Effect of $POCl_3$ Gettering Time on Ingot W134Ti009

TABLE 4

SOLAR CELL PARAMETERS AND DERIVED LIFETIMES AFTER $POCl_3$ GETTERING OF INGOT - W137 (2.1×10^{14} cm^{-3} Ti)

Gettering Condition	Uncoated Efficiency (%)	I_{sc} (mA)	τI_{SC} (μsec)
No gettering	4.24	12.63	0.103
950°C, 1 hr.	4.23	12.70	0.105
1000°C, 1 hr.	4.55	13.60	0.141
1100°C, 1 hr.	4.87	14.10	0.167
1100°C, 2 hrs.	5.00	14.50	0.192
1100°C, 3 hrs.	5.19	14.80	0.213
1100°C, 3 hrs.	5.49	15.40	0.262

TABLE 5

SOLAR CELL PARAMETERS AND DERIVED LIFETIMES AFTER $POCl_3$ GETTERING OF INGOT - W134 (5×10^{13} cm^{-3} Ti)

Gettering Condition	Uncoated Efficiency (%)	I_{sc} (mA)	τI_{SC} (μsec)
No gettering	5.56	15.42	0.26
950°C, 1 hr.	5.30	15.36	0.258
1000°C, 1 hr.	5.69	15.68	0.289
1100°C, 1 hr.	5.99	16.20	0.35
1100°C, 2 hrs.	6.41	16.98	0.47
1100°C, 3 hrs.	6.35	17.06	0.486
1100°C, 5 hrs.	6.71	17.58	0.60

$$I_{sc} = I_{sc}(\infty) \left[\frac{1}{\frac{L_\lambda}{L_n} + 1} \right] \qquad (2)$$

Substituting $L = \sqrt{D\tau}$ = we get

$$\tau = \frac{L_\lambda^2}{D} \left[\frac{1}{\frac{I_{sc}(\infty)}{I_{sc}} - 1} \right]^2 \qquad (3)$$

$I_{sc}(\infty)$ is the short-circuit current for infinite diffusion length in the base = $1.08 \cdot I_{sc}(bL)$ = 24.3 mA. Using $I_{sc}(\infty)$ of 24.3 mA, D of 33 cm^2/sec and L_λ = 17 μm Equation (3) is reduced to

$$\tau = 8.76 \times 10^{-8} \left[\frac{1}{\frac{24.3}{I_{sc}} - 1} \right]^2 \qquad (4)$$

Substituting the measured I_{sc} values in Equation (4), we calculate the lifetimes for the gettered cells. These results, shown in the third column of Tables 4 and 5, indicate that the most intense gettering condition used so far (five hours at 1100°C) improves the lifetime by a factor of ∿ 2.5 in both of the Ti-doped ingots. Since $\tau \propto 1/N_T$, $\propto 1/N_X$, it appears that intense gettering reduced the Ti recombination center density (N_T) or the net impurity content in silicon (N_X) by a factor of ∿ 2.5.

3.2.2.2 Deep Level Transient Spectroscopy of Gettered Material

Deep level transient spectroscopy has been performed on the gettered solar cells fabricated from ingot W137Ti010 to quantitatively assess the conclusions drawn from the I-V and cell data and to demonstrate that $POCl_3$ gettering actually reduces the Ti concentration as

we have hypothesized. Solar cells from each gettering condition have been reprocessed for the DLTS measurements. The front metal grid was removed and in its place a Ti-Au contact was evaporated. Mesa dots 30 mils in diameter were then delineated by the photoresist technique. Previously we reported[1,5] that Ti produces two deep levels in silicon at E_V + 0.3 eV and at E_c - 0.27 eV, respectively. It was difficult to detect the E_c - 0.27 eV level in ingot W137. Therefore, the data we report here are for the more easily observed E_V + 0.3 eV center.

From Figure 8 and the data in Table 6 it is evident that the same trap level was detected in all the gettered samples, but that the trap concentrations (N_T) were quite different for different gettering cycles. These results also illustrate how effective DLTS is for resolving changes in N_T due to gettering. (It is important to recognize that the ungettered samples also go through 825°C, 50 min $POCl_3$ diffusion which can result in gettering of some Ti. This point is being investigated by the DLTS measurements on the ungettered solar cells and the starting wafers. The DLTS on the as-grown wafers will be performed by fabricating a Schottky barrier.)

It is quite clear from Figure 8 that the active Ti concentration gradually diminishes as a consequence of the increased gettering time or the temperature. The trap density diminishes by a factor of 2 when the gettering temperature is raised from 950°C to 1100°C (gettering time 1 hr). Another factor of 2 reduction in N_T is realized when the gettering time is extended from 1 to 5 hrs at 1100°C). Thus a factor of 4 reduction in N_T was obtained by increasing the gettering intensity from 950°C/1 hr to 1100°C/5 hrs. This compares to a factor of 2.5 deduced from the lifetime ($\tau_{I_{sc}}$). This is very good agreement considering the accuracy of various measurements (N_T, I_{sc} etc) and of the modelling analysis (I_{sc} vs τ).

One must also recognize that the DLTS measurement gives the trap concentration near the junction region. This may not accurately represent the bulk material if gettering is diffusion limited and there is a variation in trap concentration between the bulk and the surface. If such a concentration profile exists, then the DLTS data will reflect

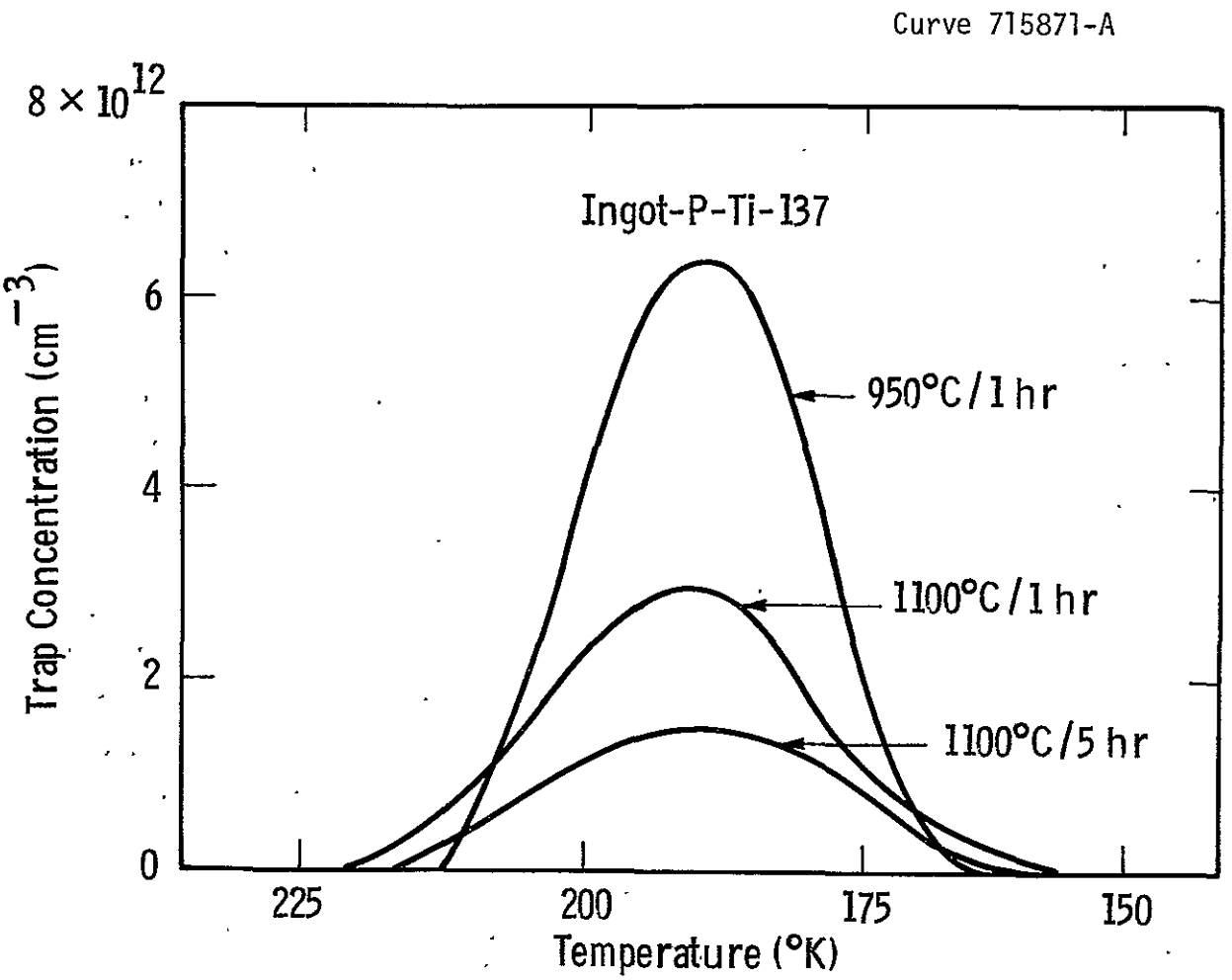

Figure 8 Effect of Gettering Condition on the Peak Amplitude (or Trap Concentration) of the E_V + 0.3 eV Trap Obtained from the DLTS Spectrum

TABLE 6

Variation in Cell Efficiency and Trap Concentration (N_T) as a Function of Gettering Treatment for Ingot W137 (original metallurgical Ti concentration, 5×10^{13} cm^{-3})

Gettering Condition	Uncoated Efficiency (%)	$E_V + 0.3$ eV N_T (cm^{-3})
No gettering	4.24	
950°C, 1 hr.	4.23	6.35×10^{12}
1000°C, 1 hr.	4.55	3.94×10^{12}
1100°C, 1 hr.	4.87	2.99×10^{12}
1100°C, 2 hrs.	5.00	2.5×10^{12}
1100°C, 3 hrs.	5.19	2.39×10^{12}
1100°C, 5 hrs.	5.49	1.49×10^{12}

the active titanium concentration at a particular location in the sample. However, this value of N_T may still be proportional to the total active Ti concentration in the bulk (N_T^1). Some experiments are being planned to determine whether or not a profile in N_T is present in the gettered samples. This will be accomplished by sequential etching followed by DLTS measurements using Schottky Barrier diodes fabricated on the etched steps.

Figure 9 illustrates how cell efficiency of the Ti-doped wafers changes with N_T due the various gettering conditions. The efficiency decreases monotonically with the increase in the trap concentration, indicating that EV + 0.3 eV level plays a major role in controlling the cell performance. Figure 10 shows the correlation between the I_{sc}-derived bulk lifetime ($\tau_{I_{sc}}$) and the reciprocal of the trap concentration. The linear relationship between the two parameters again strongly suggests that the bulk lifetime is controlled by this trap, and that the gettering-induced improvement in cell performance is primarily due to the reduction in the trap density. Further DLTS measurements are being carried out on the gettered cells fabricated from ingot W134Ti009 (2×10^{14} cm^{-3} Ti). The preliminary results are similar to that for ingot W137.

We conclude that $POCl_3$ gettering improves the cell efficiency of devices which are performance-limited by Ti contamination of the silicon base material. The benefits of gettering increase with temperature and treatment time being maximum for the highest temperature (1100°C) and longest time (5 hours) which we employed. Under the latter conditions, an absolute efficiency improvement of over 1% (e.g, an uncoated efficiency of 6.71% vs 5.56% for the ungettered material containing 5×10^{13} cm^{-3} at Ti) was observed. From the I-V analysis and the short circuit current data this improvement can be attributed to an increase in bulk lifetime during gettering. The DLTS results show quite convincingly that $POCl_3$ treatments do not alter the type of deep level present in the Ti-doped material (E_V + 0.3 eV) but rather reduce the trap density and thus improve bulk lifetime.

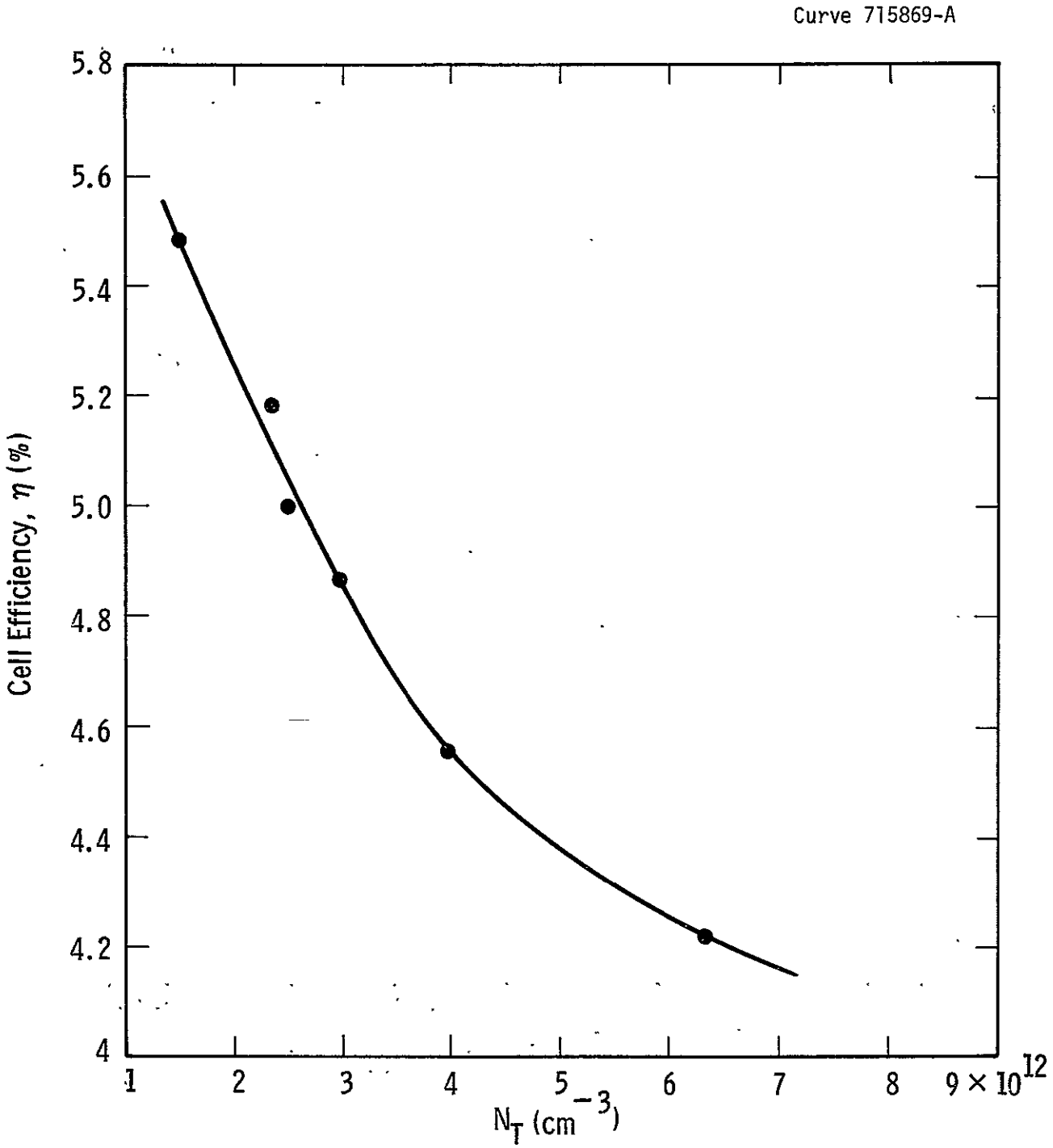

Figure 9 Solar Cell Efficiency as a Function of the Concentration of E_V + 0.30 eV Traps. These Results Were Obtained From Gettering Studies on Ingot W137Ti010

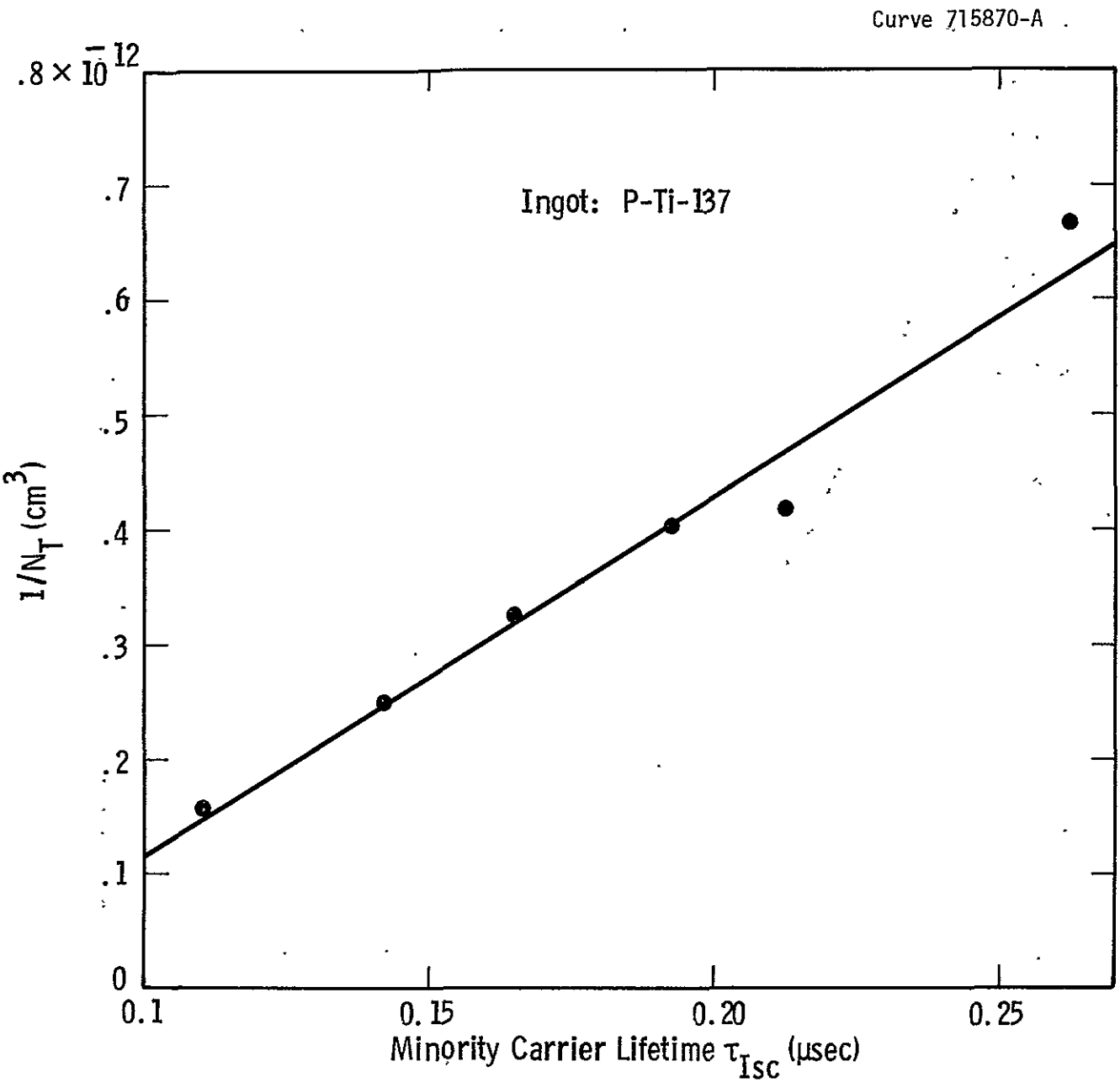

Figure 10 Minority Carrier Lifetime (Derived from Cell Short-circuit Current) as a Function the Inverse Trap Concentration of the E_V + 0.30 eV Center

3.3 Decontamination of Wafer Surfaces by Cleaning Prior to Heat Treatment

Our experience[1,6] as well as that of others[7] indicated that there are some difficulties in preserving recombination lifetime during high temperature treatments owing to wafer surface contamination. For this reason we developed a model to characterize the effects of the deionized water rinse cycle used to clean wafers[6]. We have now refined this decontamination model to account for the presence of particulate contamination on the wafer surface prior to the final deionized water rinse cycle. The origin of this contamination stems mainly from particulate matter in the H_2O_2, NH_4OH, and HCℓ chemicals used prior to the wafer rinse cycle.

The total equivalent particulate contamination on each surface per cm^2 is equal to $C_p(0) + r_p C_{pw} t$. C_{pw} is the particulate contamination in the deionized water, $C_p(0)$ is the initial surface particulate concentration and r_p is a rate constant. The total equivalent contamination on the (including soluble impurities, C_s) wafer as a function of rinse time is,[6]

$$C_{Si}(t) = C_s(0)\, e^{-r_s t} + C_p(0) + r_p C_{pw} t \qquad (5)$$

The optimum rinse time is given by,

$$t_{opt} = \frac{1}{r_s} \left\{ \ell n \left| \frac{r_s C_s(0)}{r_p C_{pw}} \right| \right\} \qquad (6)$$

Assuming complete homogeneity in the bulk volume of the wafer following high-temperature treatment, the trap concentration (N_t) will be equal to $2C_{si}(t)/h$ where h is the thickness of the wafer. The recombination lifetime, τ_r is equal to $(\sigma v_{th} N_t)^{-1}$ where σ is trap capture cross section (normally $\simeq 1\text{x}10^{-15}$ cm^2) and v_{th} is the thermal velocity of the minority carriers ($1\text{x}10^7$ cm/s). τ_r, as a function of rinse time is given by,

$$\tau_r = h \left\{ 2\sigma v_{th} \left[C_s(0)\, e^{-r_s t} + C_p(0) + r_p C_{pw}\, t \right] \right\}^{-1} \qquad (7)$$

Equation (7) was tested experimentally by varying the final deionized water-rinse time of silicon wafers and then annealing the wafers at 1000°C for 15 minutes in an atmosphere of 95% O_2 + 5% HCℓ. Following heat treatment, the silicon was slowly cooled (1°C/min.) to 200°C. At that time the specimens were manually withdrawn from the furnace.

The effect of final rinse time on τ_r is shown by the data points in Figure 11. Although the data scatter somewhat, the expected maximum in lifetime clearly occurs in the vicinity of five minutes.

The constants in Equation (7) for soluable contamination were obtained by a least squares fit to the data between 30 to 300 seconds with an initial correction for particulate contamination using judiciously chosen values of $C_p(0)$ and $r_p\, C_{pw}$. The particulate contamination constants were then obtained by a least squares fit to the data between 300 and 1380 seconds with correction for soluable contamination using the previously obtained best fit constants. The complete procedure was iterated three times to improve the fit over the entire range of times. The theoretical model parameters obtained by this best-fit method are:

$$C_s(0) = 1.97 \times 10^{11}$$

$$r_s = 4.35 \times 10^{-3}$$

$$C_p(0) = 4.34 \times 10^{10}$$

$$r_p\, C_{pw} = 2.10 \times 10^{8}$$

$$t_{opt} = 323 \text{ s.}$$

Curve 714864-A

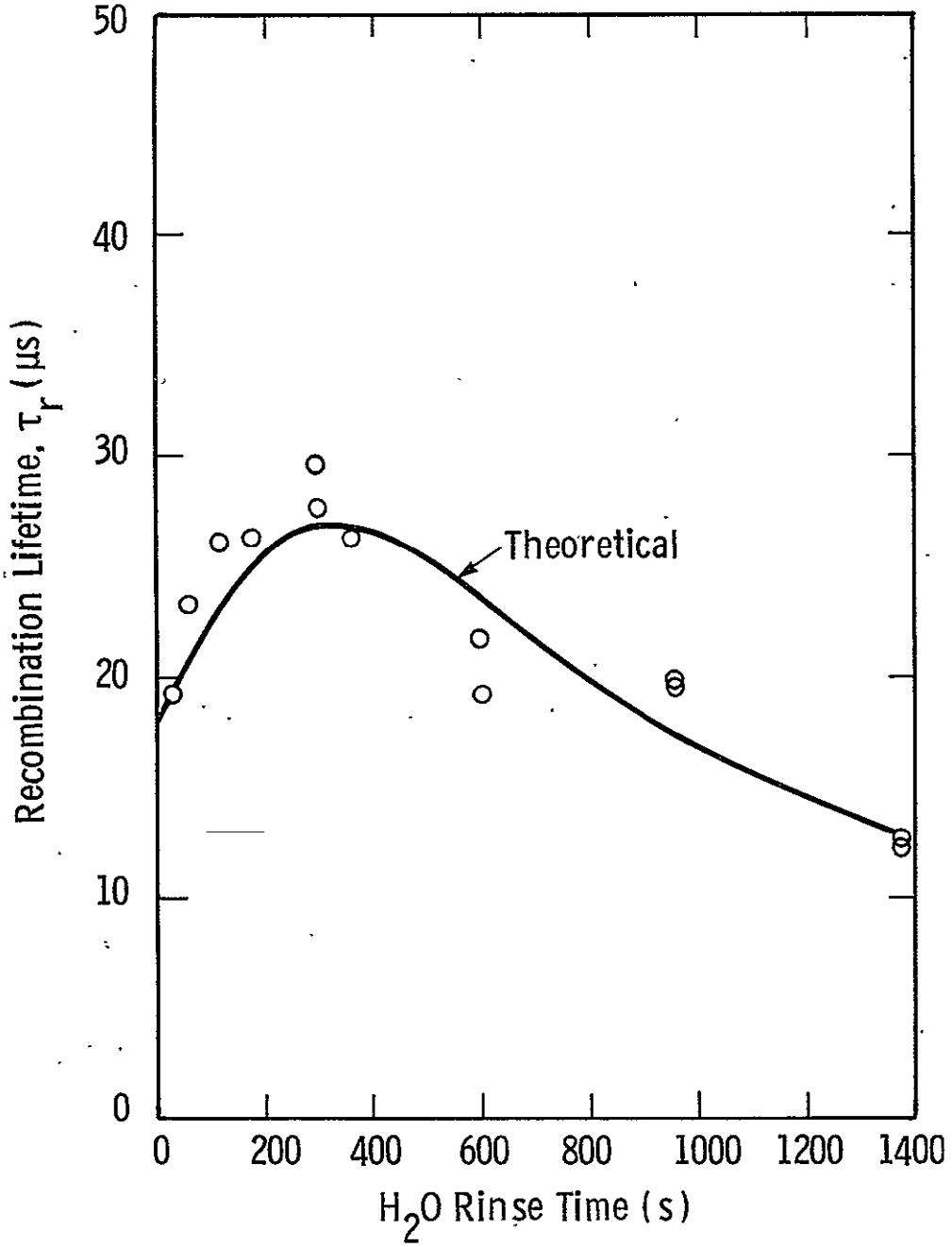

Figure 11 Experimental Data of Post Anneal Recombination Lifetime Compared to Theoretical Curve

Previous data[7] had indicated that the maximum lifetime after the high temperature treatment was only 15.2 μs. While only three data points were available then to determine $r_p C_{pw}$, the value obtained was 1.55×10^9. The change in the value of $r_p C_{pw}$ from that obtained earlier (1.55×10^9) to the present value of 2.10×10^8 is believed due to decreased microbial activity between summer (May 24, 1978) and winter (January 1, 1977) months, respectively, when the two sets of experiments were run. It is possible that an effect of this type might also explain the slightly differing response of the baseline wafers to the gettering treatments described in Section 3.2. The two sets of gettering experiments were performed at different times during the year. This point will be clarified in future experiments.

Equation (7) also predicts that τ_r (after high-temperature redistribution of surface contaminants) should be proportional to h, the wafer thickness. This is, in fact, the trend illustrated in Figure 12 where τ_r is plotted against wafer thickness. The model and experiment are thus in qualitative agreement. A best fit of a curve to the data points in Figure 12 gives an exponent of 2.086 compared to the theoretically expected value of unity. We ascribe the lack of quantitative agreement to inadequate redistribution of surface contaminants in the thickest samples. The experiment will be repeated with a longer heat treatment time to insure homogenous distribution of the surface impurities.

3.4 Investigation of Anisotropy Effects Due to Impurity Incorporation in 3-inch Diameter Czochralski Ingots

In the last quarterly report[4] we presented preliminary information on the variation in solar cell performance across the diameter of three inch Czochralski wafers doped with Mn or Ti. Cell efficiency and OCD lifetime were mapped in each case by means of 1cm x 1cm miniature solar cells and mesa diodes, respectively, distributed on the wafer surface. We concluded that the cell performance variation over the wafer was less than $\pm$ 10% of the mean value for both the Ti and Mn-doped ingots.

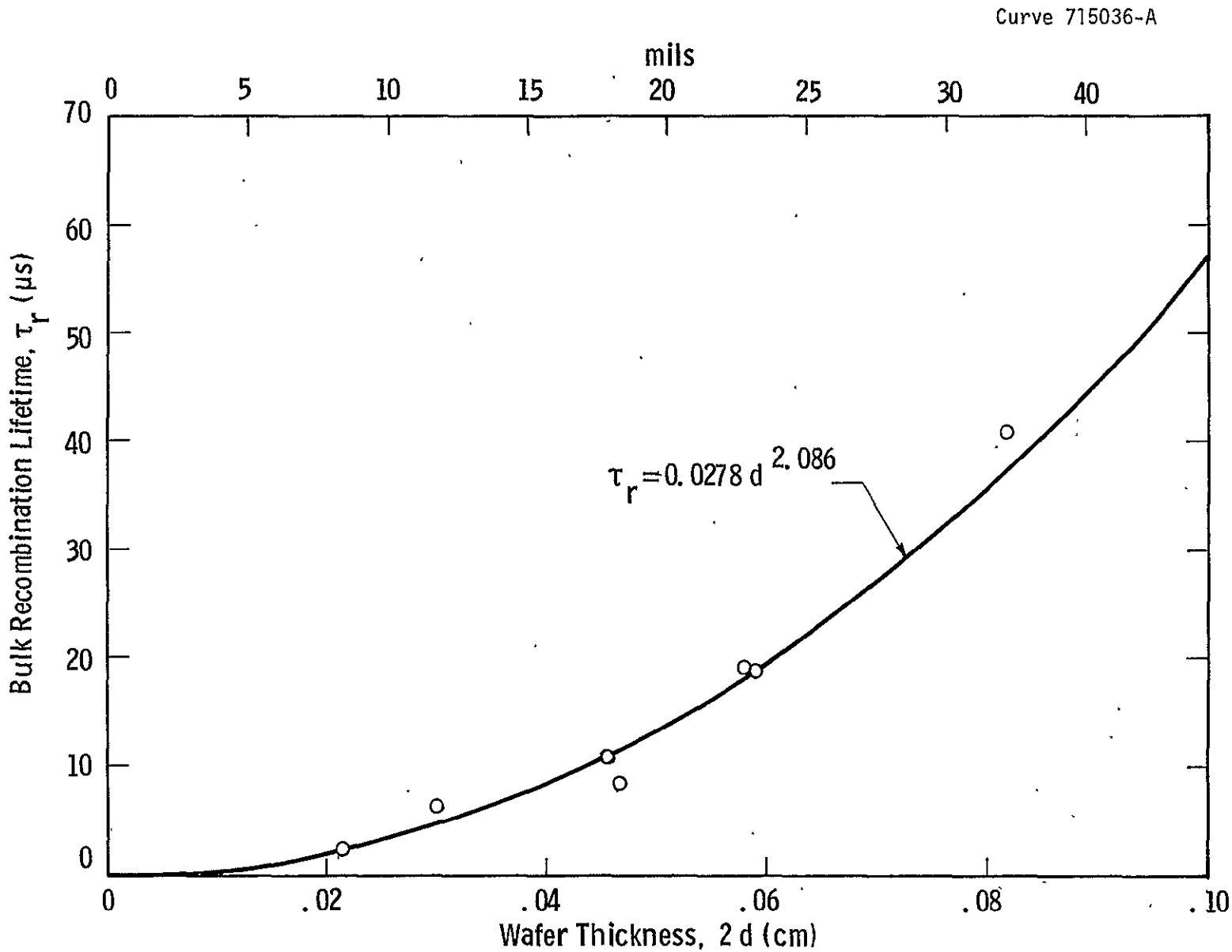

Figure 12 Effect of Wafer Thickness on Post Anneal Lifetime

Since then we have made more detailed evaluation of potential anisotropy using 6 large wafers, 3 from the (W131Mn008) Mn-ingot and the other 3 from Ti (W140Ti011) ingot. Of the 3 wafers from each ingot one was from seed, one from center, and one from the tang end. Each large wafer was scribed into quarters so larger areas could be mapped by the miniature cells. This way we were able to get as many as 22 miniature cells on each wafer as opposed to only 12 in our previous experiments. Thus, we were able to probe the center and the edge regions of the large wafers with the miniature cells. A more careful examination of seed to tang ingot property variations was also made.

Table 7 and 8 show the miniature cell performance for the Mn- and Ti-ingots, respectively. In the tables, the designations T, C and S stand for tang, center and seed. The results indicate an average uncoated cell efficiency of 8.59% with a standard deviation of 0.44 for the Mn-ingot and an average efficiency of 4.28% with a standard deviation of 0.38 for the Ti-ingot. Thus, as before in both cases most of the cells were within $\pm$ 10% of the mean value, implying no striking anisotropy overall. There does appear to be a slight systematic decrease in efficiency of cells from the tang and wafers compared to those from the seed. This is particularly evident for the Ti-doped ingot, Table 8. This might be expected since some impurity segregation will occur during growth.[1]

A few cells (marked by asterik in Tables 7 and 8) exhibited unusually low cell efficiency. A close look at the data for these devices reveals that they contain process-induced faults, such as high resistance (R), high or excess junction leakage, or shunting (high N value). The data for these cells were not used in estimating the mean values. The short-circuit currents of the poor cells are not very different from the good ones, implying that the lifetime (or the impurity content) of these cells is very similar to the rest of the devices. Thus the actual anisotropy in the impurity distribution is responsible for not more than a $\pm$ 10% deviation from the average miniature cell performance, any exceptions being due to the process effects.

TABLE (7)

Miniature Solar Cell Data for Ingot W131Mn008

81212A W131MN008 T.~ee Inch W117 00 000
SOL11 1/29/79 AM1: PO=91.60MW/CM 2 NO AR Coating

ID	ISC	VOC	IP	LOG(IO)	N	R	FF	EFF	OCD	PCDA	PCDB
1B	21.60	.556	19.63	-6.770	1.82	-.74	.747	9.49	3.64	.00	.00
2B	21.70	.556	19.71	-6.721	1.84	-.81	.748	9.54	3.90	.00	.00
3B	21.60	.555	19.43	-6.302	2.00	-.78	.730	9.26	3.90	.00	.00
4B	21.70	.554	19.71	-6.703	1.84	-.81	.747	9.50	3.64	.00	.00
5B	21.70	.553	19.60	-6.343	1.97	-1.15	.744	9.45	3.64	.00	.00
6B.*	21.50	.553	17.85	-3.766	4.39	-5.85	.683	8.58	3.25	.00	.00
>THIS IS INGOT W138MN008											
1C	20.50	.542	18.52	-6.617	1.84	-.47	.732	8.60	1.30	.00	.00
2C.*	19.80	.527	14.99	-3.011	6.63	-8.47	.589	6.50	.29	.00	.00
3C	20.60	.543	18.76	-7.044	1.69	-.29	.741	8.77	1.56	.00	.00
4C	20.50	.540	18.49	-6.471	1.89	-.64	.732	8.57	1.30	.00	.00
5C	20.70	.537	17.50	-4.451	3.24	-2.29	.661	7.77	.91	.00	.00
6C.*	19.30	.509	14.11	-5.255	2.40	9.11	.429	4.45	.13	.00	.00
7C	20.70	.543	18.73	-6.740	1.79	-.24	.730	8.67	1.43	.00	.00
8C.*	19.70	.523	14.81	-3.185	5.85	-5.02	.554	6.04	.39	.00	.00
9C	20.80	.542	18.84	-6.766	1.78	-.33	.733	8.74	1.56	.00	.00
10C	20.80	.541	18.87	-6.824	1.76	-.36	.736	8.76	1.56	.00	.00
11C	20.90	.540	18.53	-5.759	2.21	-.94	.710	8.47	1.17	.00	.00
12C	21.00	.543	19.03	-6.757	1.79	-.43	.736	8.88	1.69	.00	.00
13C	21.00	.540	18.93	-6.524	1.86	-.36	.726	8.70	1.56	.00	.00
14C	21.10	.538	18.52	-5.382	2.42	-1.29	.700	8.41	1.04	.00	.00
15C	20.70	.540	18.70	-6.544	1.86	-.66	.735	8.69	1.69	.00	.00
16C	20.80	.534	18.04	-5.061	2.64	-1.47	.685	8.05	1.30	.00	.00
17C	20.90	.540	18.98	-6.824	1.75	-.54	.742	8.86	2.21	.00	.00
18C	20.90	.534	18.16	-5.160	2.56	-1.20	.684	8.07	.13	.00	.00
19C	20.90	.543	18.97	-6.879	1.74	-.30	.737	8.84	1.56	.00	.00
20C	21.10	.540	18.80	-5.921	2.12	-.92	.717	8.65	1.30	.00	.00
21C.*	19.60	.526	14.90	-3.243	5.68	-5.13	.566	6.17	.34	.00	.00
22C	20.90	.539	18.79	-6.337	1.93	-.61	.726	8.65	1.30	.00	.00
1T	21.00	.545	18.95	-6.496	1.89	-.61	.732	8.86	1.95	.00	.00
2T	20.80	.543	18.72	-6.372	1.93	-.69	.729	8.71	1.95	.00	.00
3T	21.30	.546	19.28	-6.700	1.81	-.37	.733	9.01	1.95	.00	.00
4T	21.00	.544	19.08	-6.866	1.75	-.48	.742	8.96	2.08	.00	.00
5T	20.70	.541	18.39	-5.772	2.21	-1.14	.716	8.48	1.82	.00	.00
6T	20.70	.541	18.79	-6.823	1.76	-.44	.739	8.75	1.04	.00	.00
7T	20.70	.539	18.78	-6.761	1.77	-.54	.740	8.73	1.04	.00	.00
8T	20.80	.521	17.44	-4.467	3.12	-1.41	.640	7.33	.40	.00	.00
9T	20.60	.538	18.72	-6.945	1.71	-.29	.738	8.65	1.30	.00	.00
10T	20.60	.539	18.73	-7.000	1.69	-.19	.737	8.65	1.30	.00	.00
11T	20.20	.536	18.18	-6.463	1.88	-.41	.724	8.29	1.30	.00	.00
12T	20.20	.536	18.13	-6.284	1.95	-.64	.724	8.28	1.04	.00	.00
13T	20.50	.535	18.14	-5.712	2.22	-.95	.707	8.20	.91	.00	.00
14T	20.90	.536	18.62	-5.939	2.10	-.84	.716	8.48	1.04	.00	.00
15T	20.50	.527	17.64	-4.850	2.78	-1.75	.678	7.75	.91	.00	.00
16T	20.80	.510	17.37	-4.546	2.97	-.59	.624	7.00	.91	.00	.00
17T	20.50	.532	17.72	-4.913	2.76	-1.91	.687	7.92	.65	.00	.00
19T	20.50	.537	19.81	-17.147	.58	1.29	.828	9.64	1.17	.00	.00

TABLE (7) (Cont.)

ID	ISC	VOC	IP	LOG(10)	N	R	FF	EFF	OCD	PCDA	PCDR
1S	21.40	.543	19.28	-6.461	1.89	-.51	.728	8.95	1.70	.00	.00
2S	20.80	.542	18.30	-5.481	2.38	-1.19	.702	8.37	1.70	.00	.00
3S	21.60	.545	19.59	-6.797	1.77	-.35	.736	9.16	1.70	.00	.00
4S	21.60	.547	19.45	-6.383	1.94	-.60	.729	9.10	2.21	.00	.00
5S	20.30	.543	18.14	-6.049	2.08	-.88	.720	8.40	1.69	.00	.00
6S	21.20	.546	19.09	-6.426	1.92	-.53	.727	8.90	1.95	.00	.00
7S	21.30	.543	19.18	-6.422	1.91	-.55	.728	8.91	.70	.00	.00
8S	20.50	.536	17.91	-5.217	2.54	-1.61	.698	8.11	.65	.00	.00
9S	20.90	.540	18.63	-5.873	2.15	-1.16	.722	8.62	1.30	.00	.00
10S	21.00	.541	19.03	-6.713	1.79	-.56	.739	8.88	1.56	.00	.00
11S	20.90	.540	18.80	-6.359	1.93	-.64	.728	8.69	1.43	.00	.00
12S	21.00	.540	18.62	-5.700	2.24	-1.16	.714	8.56	1.43	.00	.00
13S	21.20	.540	18.90	-5.888	2.14	-1.11	.722	8.74	1.56	.00	.00
14S	21.20	.541	18.95	-5.989	2.09	-1.02	.724	8.78	1.04	.00	.00
15S	20.70	.544	18.89	-7.162	1.66	-.30	.746	8.88	2.08	.00	.00
16S	21.10	.541	19.21	-6.991	1.70	-.42	.745	8.99	1.95	.00	.00
17S	21.00	.543	19.12	-6.987	1.71	-.39	.743	8.96	1.82	.00	.00
18S	21.10	.543	19.15	-6.795	1.77	-.49	.740	8.96	2.08	.00	.00
19S	21.30	.539	19.12	-6.228	1.98	-.76	.727	8.82	1.69	.00	.00
AVERAGES: 81212A BASELINE W117 00 000											
	21.66	.555	19.62	-6.568	1.89	-.86	.743	9.45	3.74	.00	.00
STD	.05	.001	.10	.202	.08	.15	.007	.10	.13	*	*
81212A W132MN008 THREE INCH											
	20.86	.539	18.67	-6.401	2.03	-.72	.722	8.59	1.41	.00	.00
STD	.31	.006	.53	1.625	.42	.53	.029	.44	.46	*	*
PERCENT OF BASELINE											
	96.3	97.2	95.2	102.5	107	116.1	97.1	91.0	37.7	*****	*****
STD%	1.6	1.3	3.2	28.5	28	87.5	4.8	5.7	13.9	*****	*****

TABLE (8)

Miniature Solar Cell Data for Ingot W140Ti011

81212 W140T1011 Three Inch W117 00 000
SOL11 1/29/79 AM1: PO-91.60MW/CM 2 NO AR Coating

ID	ISC	VOC	IP	LOG(IO)	N	R	FF	EFF	OCD	PCDA	PCDB
2R*	21.90	.559	19.52	-5.727	2.30	-1.60	.730	9.45	.00	.00	.00
1B	22.40	.555	20.52	-7.380	1.62	-.17	.750	9.86	4.55	.00	.00
2B	21.60	.555	19.57	-6.640	1.86	-.70	.741	9.40	3.25	.00	.00
3B.*	21.90	.551	19.25	-5.361	2.49	-1.44	.706	9.00	3.90	.00	.00
4B	22.30	.553	20.32	-7.040	1.71	-.32	.744	9.70	4.81	.00	.00
5B	22.10	.552	19.97	-6.571	1.88	-.49	.733	9.46	4.55	.00	.00
6B	22.50	.553	20.66	-7.626	1.55	.06	.749	9.86	4.81	.00	.00
>THIS IS W140TI011											
1T	11.40	.471	10.39	-7.860	1.33	1.45	.720	4.09	1.04	.00	.00
2T	11.40	.468	10.32	-7.387	1.44	1.07	.714	4.03	.91	.00	.00
3T	11.30	.465	10.27	-7.603	1.37	1.08	.720	4.00	.15	.00	.00
4T	11.80	.469	10.54	-6.679	1.65	.64	.698	4.08	.91	.00	.00
5T	11.60	.476	10.58	-7.900	1.33	1.43	.722	4.21	1.30	.00	.00
6T	10.60	.460	9.41	-6.401	1.74	.14	.695	3.58	.78	.00	.00
7T.*	10.70	.429	6.94	-4.524	2.81	15.71	.368	1.79	.20	.00	.00
8T	10.50	.458	9.19	-5.733	2.04	-1.23	.686	3.49	1.04	.00	.00
9T	11.20	.465	9.98	-6.566	1.68	.43	.697	3.84	.91	.00	.00
10T	11.60	.470	10.53	-7.477	1.42	1.00	.718	4.14	1.04	.00	.00
12T	11.40	.469	10.29	-7.128	1.51	.66	.713	4.03	1.04	.00	.00
14T	11.00	.463	9.91	-7.093	1.51	.91	.707	3.81	.91	.00	.00
15T	11.10	.462	10.00	-7.115	1.50	1.03	.706	3.83	.65	.00	.00
16T	10.70	.453	9.19	-5.346	2.24	-.80	.656	3.37	.91	.00	.00
17T	10.80	.462	9.70	-6.940	1.55	.75	.705	3.72	.91	.00	.00
18T	10.70	.456	9.45	-6.265	1.77	.46	.683	3.52	.91	.00	.00
19T.*	11.00	.426	6.97	-2.998	6.60	-3.07	.409	2.03	.20	.00	.00
20T.*	10.80	.442	7.59	-2.978	7.02	*****	.518	2.62	.40	.00	.00
21T	11.20	.451	9.73	-5.778	1.97	.41	.661	3.53	.65	.00	.00
22T	11.50	.462	10.09	-5.993	1.90	.27	.675	3.79	.78	.00	.00
23T	11.20	.461	10.04	-6.868	1.57	.86	.700	3.82	.91	.00	.00
1C	12.00	.478	10.91	-7.638	1.40	1.19	.719	4.36	1.04	.00	.00
2C	12.20	.477	11.05	-7.413	1.45	1.15	.713	4.39	1.04	.00	.00
3C	12.30	.477	11.10	-7.177	1.51	1.01	.708	4.39	.91	.00	.00
4C	12.10	.477	11.00	-7.666	1.39	1.29	.717	4.38	.91	.00	.00
5C	12.40	.475	11.11	-6.886	1.59	1.10	.696	4.34	1.04	.00	.00
6C.*	11.60	.429	7.02	-3.997	3.47	14.73	.341	1.79	.91	.00	.00
7C	12.10	.475	10.99	-7.516	1.42	1.05	.718	4.36	1.04	.00	.00
8C	12.50	.474	11.25	-6.935	1.57	.52	.710	4.45	.91	.00	.00
9C	12.20	.474	11.04	-7.378	1.45	1.15	.712	4.35	.91	.00	.00
10C	12.20	.474	11.04	-7.378	1.45	1.15	.712	4.35	.91	.00	.00
11C	12.20	.474	10.97	-7.045	1.54	1.13	.701	4.29	1.04	.00	.00
12C	12.40	.478	11.24	-7.452	1.44	1.15	.714	4.47	.16	.00	.00
13C	12.40	.475	11.21	-7.357	1.46	1.38	.706	4.40	1.30	.00	.00
14C	12.10	.476	11.00	-7.654	1.39	1.29	.717	4.37	.91	.00	.00
15C	12.10	.477	11.00	-7.666	1.39	1.29	.717	4.38	1.04	.00	.00

TABLE (8) (Cont.)

ID	ISC	VOC	IP	LOG(10)	N	R	FF	EFF	OCD	PCDA	PCDB
16C	12.40	.475	11.13	-6.826	1.61	.61	.704	4.39	.91	.00	.00
17C	12.20	.473	10.95	-6.929	1.58	.88	.702	4.28	1.04	.00	.00
19C	11.90	.474	11.20	-10.932	.88	2.01	.768	4.58	.78	.00	.00
20C	12.40	.459	11.43	-8.913	1.09	2.23	.725	4.36	.78	.00	.00
21C	12.10	.473	11.36	-10.507	.92	1.81	.765	4.63	.91	.00	.00
22C	12.00	.474	11.31	-11.247	.85	2.15	.769	4.63	1.04	.00	.00
1S	12.40	.475	11.46	-8.812	1.15	1.49	.741	4.62	.91	.00	.00
2S	12.30	.471	11.42	-9.518	1.03	2.09	.742	4.54	.91	.00	.00
3S	12.70	.475	11.86	-9.955	.98	1.84	.754	4.81	.91	.00	.00
4S.*	11.80	.442	8.00	-3.239	5.55	-1.51	.446	2.46	.91	.00	.00
5S	12.40	.475	11.62	-10.484	.93	2.05	.759	4.73	.16	.00	.00
6S	12.60	.480	11.72	-9.330	1.08	1.37	.754	4.82	.91	.00	.00
7S	12.50	.478	11.74	-10.674	.91	1.99	.763	4.82	.91	.00	.00
8S	12.60	.477	11.78	-9.985	.99	1.66	.759	4.83	1.04	.00	.00
9S	12.40	.477	11.50	-9.295	1.08	2.00	.740	4.63	.00	.00	.00
11S	12.60	.476	11.78	-9.968	.99	1.66	.759	4.81	.00	.00	.00
12S	12.70	.469	11.68	-8.441	1.20	1.48	.732	4.61	.00	.00	.00
13S	12.00	.470	9.94	-4.561	2.97	-2.02	.624	3.72	.00	.00	.00
14S	12.80	.476	11.53	-7.058	1.54	.82	.708	4.56	.00	.00	.00
15S	13.30	.480	11.85	-6.590	1.70	.93	.689	4.65	.91	.00	.00
16S.*	12.60	.469	10.56	-4.574	2.93	-3.06	.648	4.05	.30	.00	.00
17S	12.70	.476	11.33	-6.489	1.73	.13	.702	4.48	.80	.00	.00
18S	12.90	.475	11.48	-6.385	1.76	.07	.699	4.53	.78	.00	.00
19S.*	12.60	.469	10.18	-3.917	3.88	-5.90	.625	3.91	.39	.00	.00
20S	12.80	.474	11.49	-6.868	1.59	.69	.704	4.52	.91	.00	.00
21S	12.70	.475	11.38	-6.767	1.63	.60	.702	4.48	.91	.00	.00
22S	12.70	.472	11.12	-5.767	2.04	-.54	.682	4.32	.91	.00	.00
23S	12.60	.472	11.25	-6.502	1.71	.12	.702	4.42	.78	.00	.00
24S.*	12.70	.475	9.71	1.077	****	*****	****	*****	.91	.00	.00
AVERAGES: 81212 BASELINE W117 00 000											
	22.18	.554	20.21	-7.052	1.72	-.32	.743	9.65	4.39	.00	.00
STD	.32	.001	.39	.410	.13	.26	.006	.20	.58	*	*
81212 W140TI011 AND W131MN008 THREE INCH											
	12.02	.471	10.87	-7.616	1.47	.96	.714	4.28	.81	.00	.00
STD	.66	.007	.72	1.476	.37	.81	.028	.38	.33	*	*
PERCENT OF BASELINE											
	54.2	85.1	53.8	92.0	85	494.9	96.0	44.3	18.4	*****	*****
STD%	3.8	1.4	4.7	28.4	30	683.5	4.6	4.9	10.8	*****	*****

Figures 13 and 14, respectively show the miniature cell efficiency map on tang, center and seed wafers from the 3 inch diameter Mn and Ti-ingots. Neglecting those cells which were affected by the process, the maps illustrate the small variation in the cell performance across the wafers suggested by the data in Tables 7 and 8. There are no regions of the wafers where cell efficiency falls significantly above or below and the performance average. We conclude that the observed variation in the cell performance is random across the wafer, not anisotropic. Some seed to tang performance shift is evident in Figure 14 as noted above.

Since solar cell performance is the net result of process as well as impurity effects the miniature cell efficiency map by itself may not provide all the information required to delineate the anisotropy in the impurity distribution. Moreover, the cell efficiency is only an indirect measure of the impurity concentration. The bulk lifetime, on the other hand, is inversely proportional to the trap concentration for the impurity induced deep level. (See Section 3.2) In turn, the deep level concentration is porportional to the total impurity content in the cell as follows :

$$\tau \propto \frac{1}{\sigma N_t V_{th}} \propto \frac{1}{N_t} \propto \frac{1}{N_x} \qquad (8)$$

The OCD lifetime numbers are not sufficiently accurate (about a factor of 2 in accuracy) to delineate small variations in the impurity concentration. The OCD lifetime is influenced by the junction leakage and surface recombination effects. Short-circuit current, however, is relatively insensitive to most of the process induced effects and is also a good indicator of bulk lifetime. We can, therefore, deduce a more accurate lifetime from the short circuit current using Equation 4 and the procedure outlined in Section 3.2.

Dwg. 7691A54

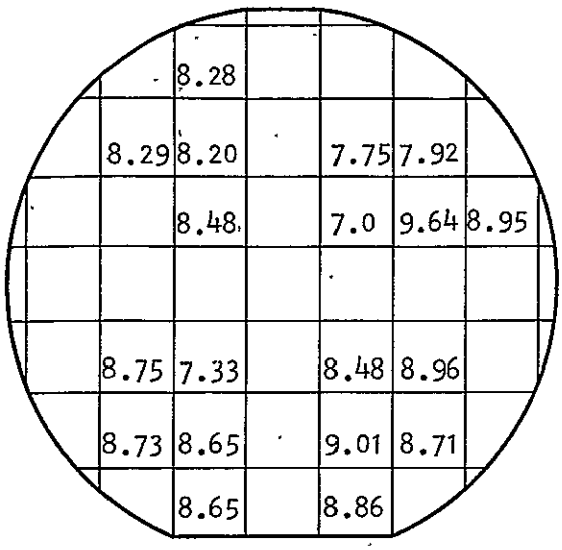

Tang

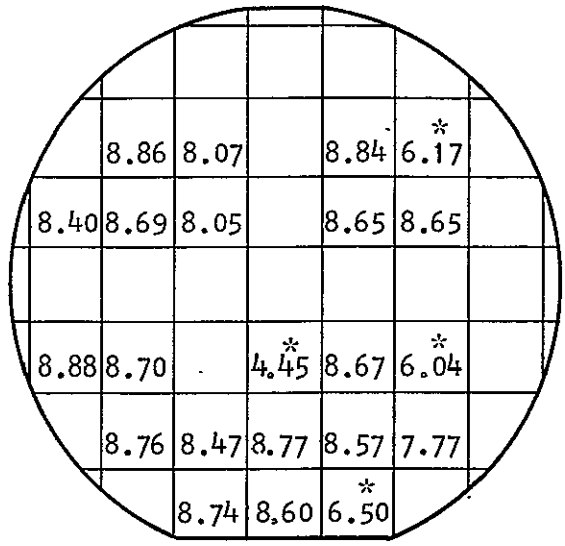

Center

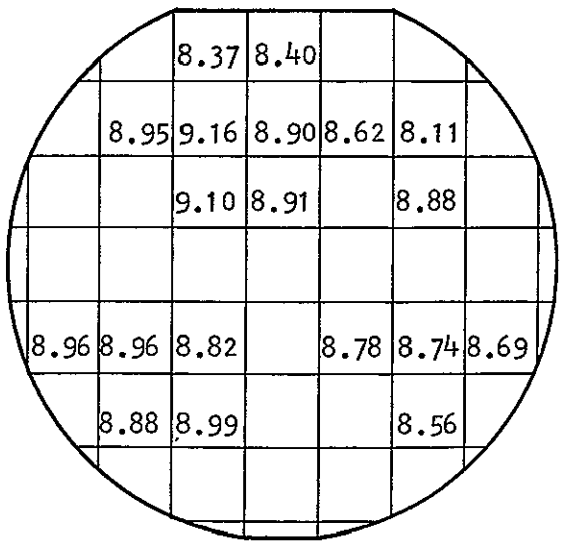

Seed

Figure 13 Cell Efficiencies (%) for Miniature Solar Cells Distributed Across 3 Inch Diameter Mn-doped Wafers Taken from Tang, Center, and Seed End

Dwg. 7691A55

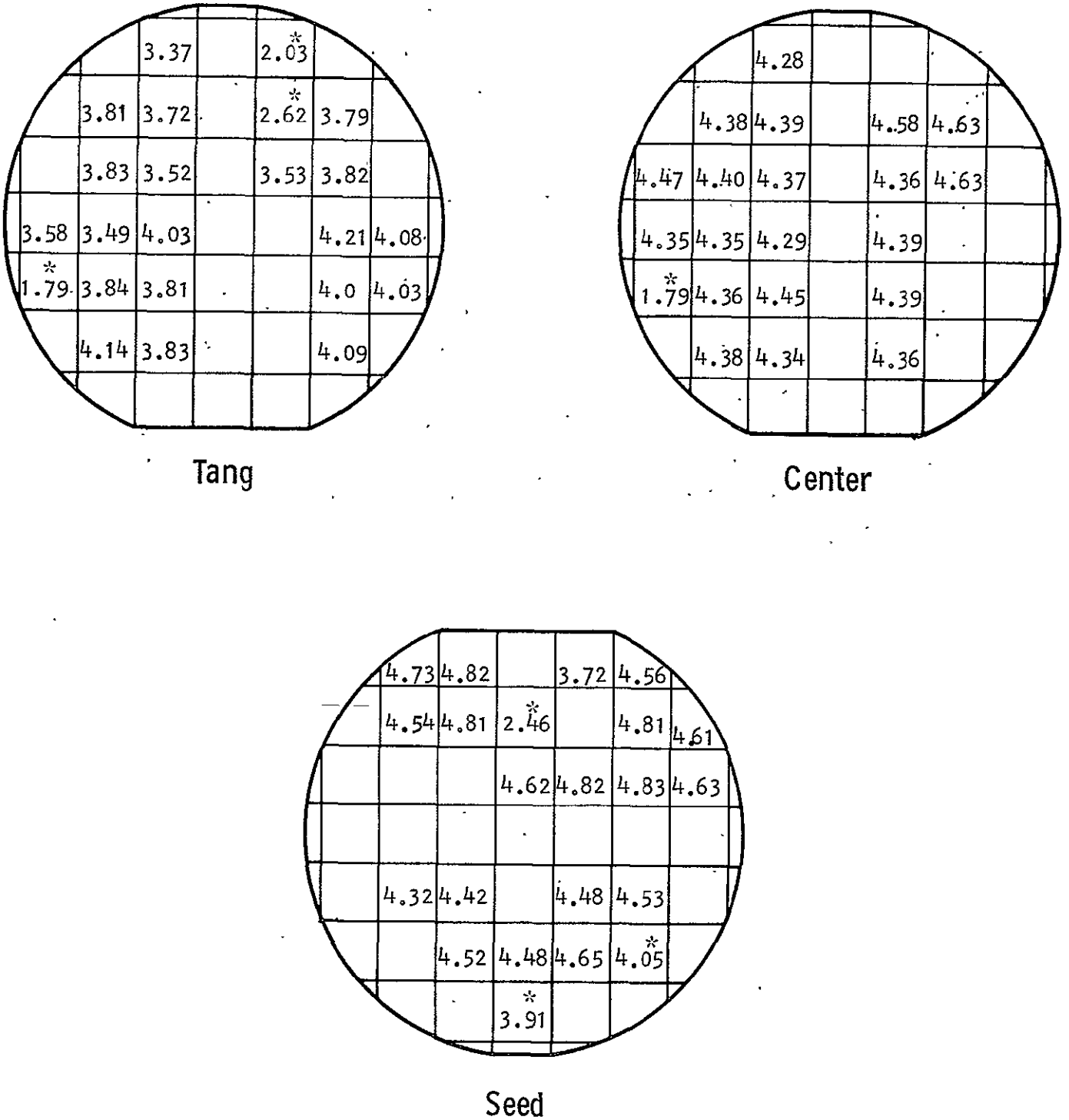

Figure 14 Cell Efficiencies (%) for Miniature Solar Cells Distributed Across 3 Inch Diameter Ti-doped Wafers Taken From Tang, Center, and Seed End

The lifetimes were calculated for the miniature cells from their measured I_{SC}, tables 7 and 8. The lifetime maps on the center wafers of both the ingots are shown in Figure 15. The maps indicate that the lifetime varies by approximately a factor of 2 across the Mn-doped wafer and by about a factor of 1.5 for the Ti-doped wafer. There are no preferred regions of high or low lifetimes. The highest and the lowest I_{SC} in Tables 7 or 8 give lifetimes which differ by a factor of approximately 2. This also represents the total variation in the lifetime throughout the entire ingot from seed to tang end. Since lifetime is inversely proportional to the impurity concentration, (Equation 8), we conclude that total anisotropy in the impurity distribution throughout the Mn or Ti-doped 3 inch diameter ingots is random and is at most a factor of 2. This much anisotropy will induce less than $\pm$ 10% variation in the cell performance, consistent with our observations.

Dwg. 7691A53

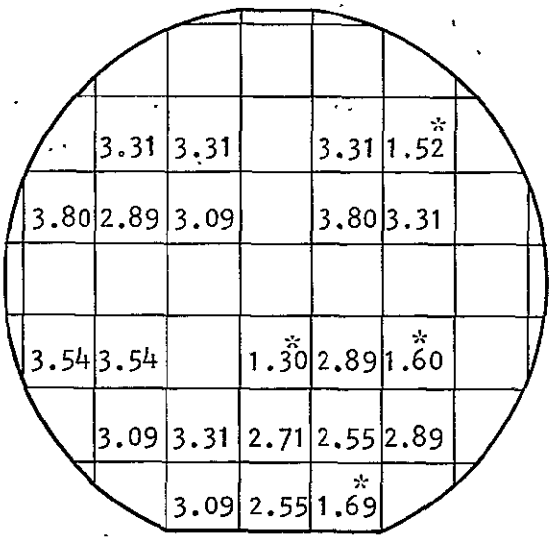

W-131 Mn - Center

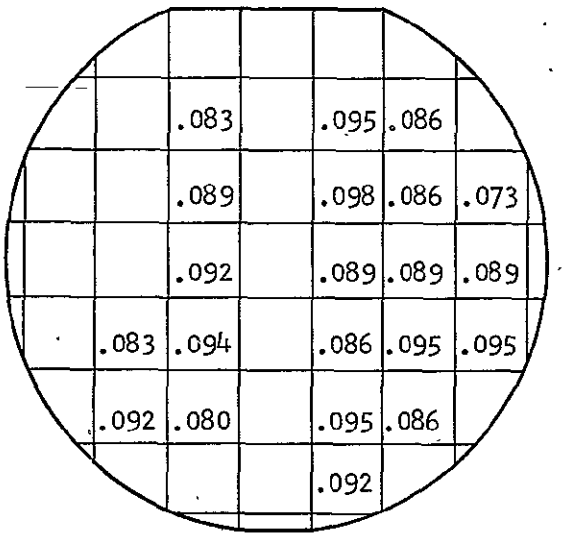

W-140 Ti - Center

Figure 15 Variation in Lifetime (Deduced From the Measured Short-Circuit Current) Across 3 Inch Diameter Mn or Ti Doped Wafer

3.5 Permanence Effects in Ti and Mo-doped Solar Cells

Solar cell arrays deployed in terrestrial applications must exhibit useful lifetimes of many years in order for photovoltaic energy systems to be economically viable. Since low cost, solar grade silicon may contain a variety of impurities, it is important to determine whether devices made on this material undergo any long term performance changes attributable to contaminant aging behavior.

To assess the permanence of the cell characteristics, we are carrying out a series of heat treatments at various times and temperatures, then measuring the cell parameters following the application of this thermal stress. The test temperatures chosen are well in excess of any temperature to which the cells will be exposed in actual service. This accelerated testing should make it possible to predict by means of appropriate models the long term behavior due to impurities.

Briefly, the experimental procedure used is as follows:[7]

1. Wafers from selected ingots are processed as a group through diffusion to the metal contacting step in the solar cell fabrication sequence.[1,6]

2. A portion of the wafers are completely processed to cells and tested; the remainder of the cells are left uncontacted.

3. The uncontacted wafers, as well as some of the contacted wafers, are subjected to a series of heat treatments for specific times. After this anneal, the uncontacted wafers are processed into completed cells.

4. The cell parameters of the heat treated samples are then compared with those of untreated samples to determine any effects of the high temperature stressing.

In selecting ingots for these tests we chose two impurities which significantly degrade the performance of silicon solar cells, Ti and Mo. Since there is a large effect due to these two impurities, we expected that cells containing Mo or Ti also would exhibit noticeable changes under stress testing if any aging effects occurred. The ingots chosen were:

W123-Ti-008 ($1x10^{14}$ Ti/cm^3)

and

W077-Mo-001 ($4.2x10^{12}$ Mo/cm^3).

Baseline ingot W097-00-000 was processed concurrently with the impurity ingots in all tests.

The following annealing cycles now have been completed:

1 hr. at 200°C
10 hrs. at 400°C
10 hrs. at 500°C
100 hrs. at 500°C
1 hr. at 800°C
10 hrs. at 800°C
100 hrs. at 800°C

The results of these first experiments are compiled in Tables 9 through 11; the effects on cell performance due to treatment at the highest temperature, 800°C, also are depicted graphically in Figure 16. Listed in the tables are the major I-V parameters for the baseline ingot and the Mo and Ti ingots both in the treated and untreated conditions. Each entry in the tables is the average of data from two to four cells. There was no large spread in the data; the results are considered statistically significant.

TABLE 9

EFFECT OF AGING AT 200 AND 400°C ON SOLAR CELL PERFORMANCE OF Mo AND Ti-DOPED SILICON

SAMPLE ID	I_{SC}(mA)	V_{OC}(V)	FF	EFF(%)+	τ_{OCD}(μsec)
● 1 HR at 200°C					
097 Base-no anneal	22.0	.550	.711	9.10	3.6
097 Base-anneal contacts	22.0	.552	.723	9.28	3.8
097 Base-anneal no contacts	21.8	.550	.767	9.71	5.3
077 Mo-no anneal	18.5	.504	.720	7.10	.7
077 Mo-anneal-contacts	18.7	.508	.726	7.29	.7
077 Mo-anneal no contacts	17.7	.500	.650	6.20	.6
123 Ti-no anneal	14.3	.480	.700	5.08	1.8
123 Ti-anneal-contacts	14.1	.484	.632	4.56	.7
123 Ti-anneal-no contacts	14.3	.481	.695	5.03	.7
● 10 HRS at 400°C					
097 Base-no anneal	22.0	.551	.732	9.38	4 4
097 Base-anneal contacts	21.7	.556	.756	9.65	4.0
097 Base-anneal no contacts	22.1	.555	.729	9.46	5.0
077 Mo-no anneal	18.9	.506	.715	7.23	.7
077 Mo-anneal-contacts	18.9	.506	.720	7.28	1.0
077 Mo-anneal no contacts	18.5	.506	.709	7.00	.6
123 Ti-no anneal	14.4	.478	.696	5.07	.7
123 Ti-anneal contacts	14.5	.484	.695	5.16	1.0
123 Ti-anneal no contacts	14.5	.485	.691	5.12	.8

*Data given are average of 2-4 cells. No large spread of data within a given treatment was noted.

+AM1; no AR coating

TABLE 10

EFFECT OF AGING ON AT 500°C ON SOLAR CELL PERFORMANCE OF Mo AND Ti-DOPED SILICON*

SAMPLE ID	I_{SC}(mA)	V_{OC}(V)	FF	EFF(%)+	τ_{OCD}(μsec)
• 10 HRS AT 500°C					
097 Base-no anneal	22.1	.555	.761	9.97	5.9
097 Base-anneal contacts	21.5	.553	.672	8.45	1.5
097 Base-anneal no contacts	22.0	.553	.752	9.66	5.9
077 Mo-no anneal	18.6	.505	.705	7.00	1.8
077 Mo-anneal contacts	18.0	.500	.662	6.30	1.8
077 Mo-anneal no contacts	18.6	.504	.711	7.02	.8
123 Ti no anneal	14.3	.478	.684	4.94	.7
123 Ti-anneal-contacts	14.3	.480	.668	4.85	.7
123 Ti-anneal no contacts	14.7	.483	.685	5.14	.7
• 100 HRS AT 500°C					
097 Base-no anneal	22.0	.553	.746	9.60	3.6
097 Base-anneal contacts	13.1	.119	-	<1	<.1
097 Base-anneal no contacts	21.6	.553	.743	9.38	5.2
077 Mo-no anneal	18.9	.503	.704	7.07	.7
077 Mo-anneal-contacts	9.4	.050	-	<1	<.1
077 Mo-anneal no contacts	18.2	.505	.709	6.89	.8
123 Ti-no anneal	14.4	.481	.698	5.11	.7
123 Ti-anneal-contacts	9.7	.071	.372	<1	<.1
123 Ti-anneal no contacts	15.0	.486	.682	5.24	.8

*Data given are average of 2-4 cells. No large spread of data within a given treatment was noted.

+AM1; no AR coating

TABLE 11

EFFECT OF AGING AT 800°C ON THE SOLAR CELL PERFORMANCE OF Mo and Ti-DOPED SILICON*

SAMPLE ID	I_{SC}(mA)	V_{OC}(V)	FF	EFF(%)+	τ_{OCD}(μsec)
• 1 HR AT 800°C					
097 Base-no anneal	22.20	.577	.727	9.85	5.0
097 Base-anneal-contacts	13.0	.08	.40	0.3	<0.1
097 Base-anneal-no contacts	22.00	.551	.736	9.40	5.0
077 Mo-no anneal	19.10	.513	.719	7.45	1.2
077 Mo-anneal-contacts	11.5	.05	.4	0.3	<0.1
077 Mo-anneal-no contacts	19.35	.504	.710	7.32	.70
123 Ti-no anneal	14.30	.484	.702	5.14	.7
123 Ti-anneal-contacts	10.0	.05	-	0.1	<0.1
123 Ti-anneal-no contacts	14.50	.479	.695	5.11	1.0
• 10 HRS AT 800°C					
097 Base-anneal-no contacts	21.35	.545	.744	9.20	6.5
077 Mo-anneal-no contacts	18.70	.500	.709	7.01	.6
123 Ti-anneal-no contacts	14.90	.479	.694	5.25	.5
• 100 HRS AT 800°C					
097 Base-anneal-no contacts	18.80	.533	.743	7.85	3.0
077 Mo-no contacts	18.70	.500	.714	7.06	.5
123 Ti-anneal- no contacts	14.50	.488	.699	5.23	.6

*Data given are averages for 2-4 cells. No large spread of data within a given treatent was noted.

+AM1; no AR coating

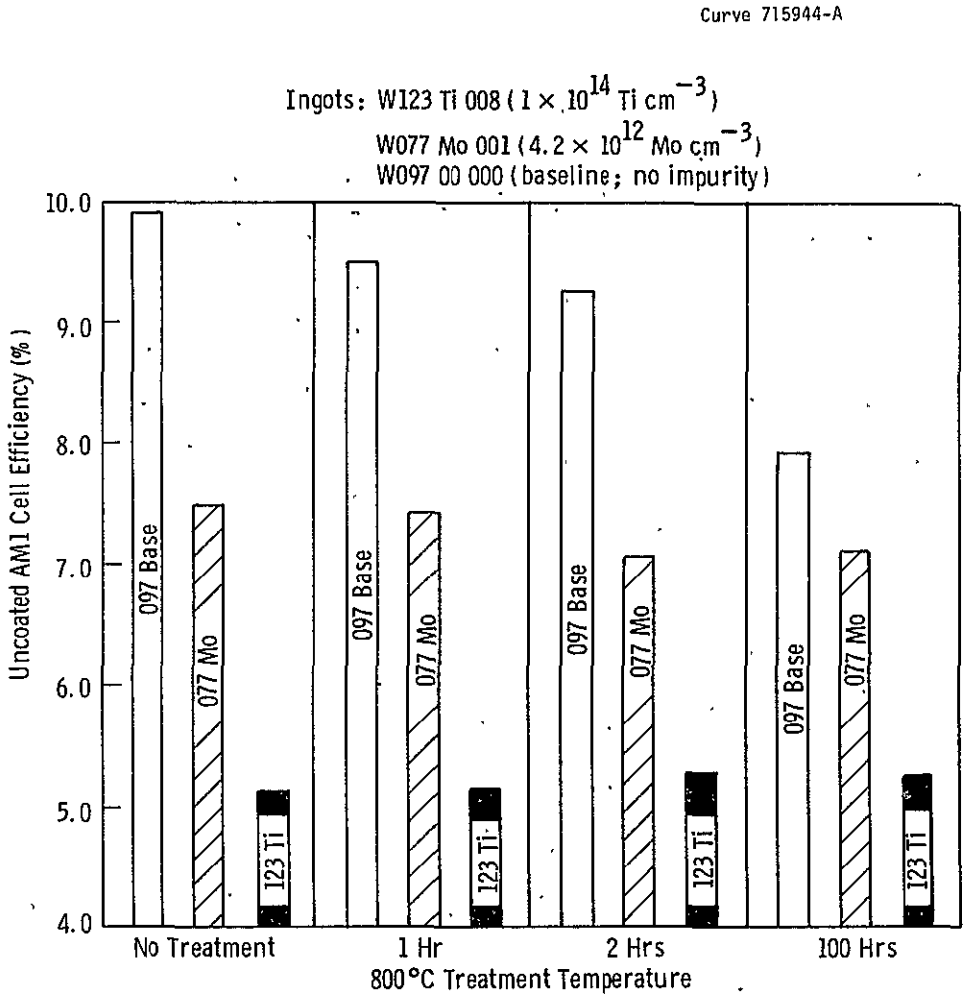

Figure 16 Effect of Aging Time at 800°C on the Performance of Uncontacted Impurity-Doped Solar Cells

On the basis of the experiments carried out so far we conclude:

1. Cells annealed with contacts in place begin to degrade after 10 hours at 500°C. This observation is consistent with our experience on contacted cells from other programs (see, for example, Reference 9). Cell performance reduction is due to the diffusion of the metal contact material through the Ti barrier layer and subsequent degradation of junction properties.

2. The baseline cells show no significant degradation up to 10 hours at 800°C, Figure 16. After 100 hours at 800°C, the baseline cell efficiency falls to about 80% of its untreated value. The efficiency reduction is due mainly to a decrease in short circuit current.

3. The Mo-doped ingot also exhibits a slight performance reduction after 100 hours at 800°C. As Figure 16 suggests, cell efficiency diminishes to about 95% of its unannealed value. Again the most evident change is a decrease in the cell short circuit current.

4. The Ti-doped ingot shows no change in cell efficiency even after 100 hours at 800°C (Figure 16), the longest time and highest temperature at which tests have been performed.

If we assume that any changes in cell parameters are due to a diffusion-controlled mechanism, the data in Tables 9, 10, and 11 can be analyzed to estimate the stability of the cells operating at a temperature near 150°C. This preliminary analysis suggests that the deployed cells would remain stable (in so far as impurity effects are concerned) for times longer than the anticipated 20 year lifetime.

3.6 Photoconductive Decay (PCD) Recombination Lifetime Measurements

As part of this program we have monitored the bulk lifetime both before and after processing of impurity-doped wafers into solar cells.[1,2] This provides a means to track any changes in properties of the as-grown material when it is subjected to further processing steps. The work had been temporarily halted during the last quarter to repair the laser used for the PCD measurements and to upgrade the measurement system somewhat. A description of recent studies as well as an updated tabulation of ingot lifetime data are given below.

3.6.1 Equipment Refinement

A new trap light was installed in the measurement apparatus (see References 1 and 2 for details) which is capable of handling a higher density of traps. The light source is a General Electric Type H7635, 160,000 CP, 50 watt, quartz halogen cycle sealed beam lamp. The output radiation, collinated by an ellipsoidal reflector, is focussed by means of an f = 1 (f.l. = 15 cm) double convex lens onto the silicon specimen. A 0.25 mm thick silicon wafer serves as a filter after the lens to eliminate visible spectrum radiation, to reduce sample heating and to promote uniform trap filling

3.6.2 PCD Measurements on Impurity-Doped Wafers

The laser-excited PCD equipment is once more operational following repolishing of the YAG:Nd laser rod and the application of new AR coatings on it. An updated summary of PCD data is compiled in Table 12 for ingots W078 to W139.

The format of the data tables has been changed somewhat from that employed previously.[1,2] Diffusion length as well as bulk recombination lifetime is now listed for each specimen, a feature reflecting the fact that diffusion length is the crucial parameter controlling carrier collection. Individual values of standard deviation have been deleted from the table, the precision of the PCD measurements having been shown to have a probable error of 5.7 percent.[1,2]

The correlation between diffusion length and solar cell short circuit current is expected to be independent of base resistivity, silicon type or method of ingot growth. Future work will explore this type of correlation.

TABLE 12

RECOMBINATION LIFETIME MEASURED BY PHOTOCONDUCTIVE-DECAY METHOD
(Q-Switched Nd: YAG Laser Excitation)

Ingot Identification	Diffusivity D_n/D_p (cm^2/s)	As Grown		Post Diffusion	
		Lifetime τ_r (μs)	Diff. Length L (μm)	Lifetime τ_r (μs)	Diff. Length L (μm)
W078-00-000	32.4	8.32	164	---	---
W079-N/00-000	11.7	86	308	---	---
W080-Ph-001	32.4	4.39	119	2.48	89.6
W081-N/Ni-001	10.5	5.62	76.8	10.36	104
W082-N/V-001	10.5	0.25	16.2	0.25	16.2
W083-N/Fe-001	11.7	1.56	42.7	---	---
W084-Al-001	32.4	0.97	56.1	1.00	56.9
W085-N/Zr-001	11.7	140	405	---	---
W086-C-001	32.0	3.06	99.0	2.30	85.8
W087-Ca-001	31.9	2.81	94.7	2.08	81.5
W088*-Cr-001	15.3	0.01	3.9	2.23	58.4
W089*-Cu-001	15.3	2.37	60.2	3.06	68.4
W090*-Mn-001	14.8	0.06	9.4	---	---
W091-Cr/Mn-002	32.4	0.09	17.1	0.20	25.5
W092-Ph-002	32.2	7.83	159	5.49	133
W093-Mn-004	32.9	0.19[3]	25.0	0.70	48.0
W094-Mn-005	32.4	0.38[3]	35.1	2.58	91.4
W095-Mn-006	32.9	0.15	22.2	0.38	35.4
W096-Mn-007	32.9	0.34[3]	33.4	2.32	87.4
W097-00-000	32.7	4.78	125	2.66	93.3
W098-Mo-002	32.4	1.40	67.3	0.89	53.7
W099-Fz-001	32.2	4.34	118	3.12	100
W100-Cu/Ti-002	32.4	0.30	31.2	0.37	34.6
W101-Fz-002	32.7	4.30	119	9.58	177
W102-Ti-006	32.9	0.21	26.3	0.29[3]	30.9
W103*-Ti-001	15.1	0.12	13.5	0.07	10.3
W104-Cu/Ti-003	33.4	0.16	23.1	0.45	38.8

Note 1.

Note 2. Insufficient electrical signal for measurement.

Note 3 Lifetime measurements subject to large errors due to extreme shallow trap density.

TABLE 12 (Cont.)

RECOMBINATION LIFETIME MEASURED BY PHOTOCONDUCTIVE-DECAY METHOD
(Q-Switched Nd: YAG Laser Excitation)

Ingot Identification	Diffusivity D_n/D_p (cm^2/s)	As Grown		Post Diffusion	
		Lifetime τ_r (μs)	Diff. Length L (μm)	Lifetime τ_r (μs)	Diff. Length L (μm)
W*105-V-001	14.8	0.07	10.2	0.07	10.2
W106-N/Al-002	11.7	16.56	139	---	---
W107-Fz/Al-001	25.0	2.61	80.8	1.65	64.2
W108-N/V-002	11.5	0.72	28.8	---	---
W109-C-002	32.4	3.05	99.4	1.72	74.7
W*110-Fe-001	13.8	Note 2	---	Note 2	---
W111-Cu/V-001	32.9	0.15	22.2	0.16	22.9
W112-Ta-001	32.4	1.06	58.6	0.68	46.9
W113-Fz/Cr-001	32.7	0.13	20.6	0.65	46.1
W114-00-000	7.5	6.75	71.2	---	---
W115-N/Cu-002	11.7	8.39	99.1	---	---
W116-Ph-001	21.7	1.61	59.1	2.40	72.2
W117-00-000	32.4	3.65	109	2.76	94.6
W118-Ph-003	26.8	4.16	106	29.3	280
W119-N/Fe-002	11.7	5,21	78.1	---	---
W120-N/Cr-002	11.6	---	---	---	---
W121-N/Ti-002	11.5	---	---	---	---
W122-Ti-007	32.2	0.68	46.8	---	---
W123-Ti-008	32.4	0.59	43.7	0.41	36.4
W124-Mo-003	32.6	1.94	79.5	2.18	84.3
W125-Mo-004	32.4	1.32	65.4	1.46	68.8
W-126-MULTI-1	32.7	0.09	17.2	0.97	56.3
W-127-FZ/TI-001	33.2	0.92	55.3	1.08	59.9
W128-TA-002	32.4	2.62	92.1	1.94	79.3
W-129-00-000	---	---	---	---	---
W130-00-000	---	---	---	---	---
W131-Mn-008	---	---	---	---	---

Note 1.

Note 2. Insufficient electrical signal for measurement.

Note 3. Lifetime measurements subject to large errors due to extreme shallow trap density.

TABLE 12 (Cont.)

RECOMBINATION LIFETIME MEASURED BY PHOTOCONDUCTIVE-DECAY METHOD
(Q-Switched Nd: YAG Laser Excitation)

Ingot Identification	Diffusivity D_n/D_p (cm^2/s)	As Grown		Post Diffusion	
		Lifetime τ_r (μs)	Diff. Length L (μm)	Lifetime τ_r (μs)	Diff. Lengt L (μm)
W-132-Ta-003	32.2	2.69	93.1	1.65	72.9
W-133-00-000	31.9	1.61	71.7	2.80	94.5
W-134-Ti-009	32.7	0.79	50.8	0.58	43.5
W-135-Fe-005	32.4	0.34	33.2	1.69	74.0
W-136-Fe-006	31.4	0.07	14.8	0.59	43.0
W-137-Ti-010	32.4	0.79	50.6	---	---
W-138-Mo-005	32.7	1.38	67.2	0.97	56.3
W-139-Mo-006	32.2	0.27	29.5	---	---
W-140-Ti-011					

Note 1.

Note 2. Insufficient electrical signal for measurement.

Note 3. Lifetime measurements subject to large errors due to extreme shallow trap density.

4. CONCLUSIONS

The response of Ti or Mo-doped solar cells to gettering treatments at temperatures up to 1100°C for times as long as 5 hours remains unaffected when the base resistivity is dropped to 0.2 Ωcm from 4 Ωcm. The efficiency of the low and high resistivity Ti-doped solar cells is improved by the gettering treatment while that of the Mo-doped cells remains unaffected by gettering. (for the ranges of parameters studied so far).

Gettering of the Ti-doped material reduces the density of recombination centers. Detailed I-V measurements indicate that as gettering time or temperature increase above 950°C the bulk lifetime of the Ti-doped material improves. This increase in bulk lifetime is inversely correlated with the concentration of trapping centers measured on the gettered material by deep level transient spectroscopy. The DLTS data convincingly show that $POCl_3$ gettering does not alter the type of deep level (E_V + 0.3 eV) present in the Ti-doped material but rather reducesthe trap density, thus improving bulk lifetime and cell performance.

Bulk lifetime (derived from I_{sc} on miniature solar cells) varies by about a factor of 2 across the diameter of 3 in. Mn-doped Czochralski ingots and by about a factor of 1.5 across a Ti-doped ingot. Similar seed to tang changes on bulk lifetime also were observed. Since lifetime is inversely proportional to impurity concentration we concluded that the total anisotropy in the impurity distribution throughout the Mn and Ti-doped ingots was at most a factor of 2. Moreover,what variation is present is randomly distributed. A change in impurity content of the size we infer would induce less than a ± 10% variation in the average cell performance, consistent with the magnitude we measured.

Ti and Mo bearing wafers heat treated at temperatures up to 800°C and times as long as 100 hours exhibit virtually no change in solar cell performance compared to the unaged value. Apparently little or no impurity-induced performance degradation occurs for these two impurities. However we did observe cell performance degradation due to interaction of the contact metal system with the base material. After 10 hours at 500°C contacted cells had essentially failed completely by this mechanism.

5. PROGRAM STATUS

The updated milestone chart is depicted in Figure 17.

5.1 Present Status

During the past quarter we:

- Prepared seventeen Czochralski ingots for further chemical, microstructural, electrical and solar cell evaluation.
- Determined the segregation coefficient of Co in silicon.
- Measured the critical Fe, W, and Co melt impurity concentrations at which single crystal structure breakdown occurs.
- Completed initial gettering experiments on low resistivity Ti and Mo doped ingots.
- Performed detailed I-V analyses and DLTS experiments to elucidate gettering mechanisms in Ti-doped silicon.
- Performed a detailed assessment of Ti and Mn impurity distributions across and along the lengths of commercial-size Czochralski ingots.
- Completed initial studies of aging (permanence) effects in Ti and Mo-doped silicon solar cells.
- Updated PCD lifetime and diffusion length measurements for as-grown and processed impurity-doped wafers.

5.2 Future Activity

During the next quarter effort will focus on (1) evaluation of HCℓ gettering to deactivate impurities in silicon solar cells (2) modeling impurity behavior in single and multiply-doped n-base silicon ingots and solar cells (3) impurity effects due to materials of construction and (4) extension of impurity aging studies to longer times and temperatures as well as other impurities.

Figure 17

PROGRAM PLAN (SCHEDULE)
(PHASE III)

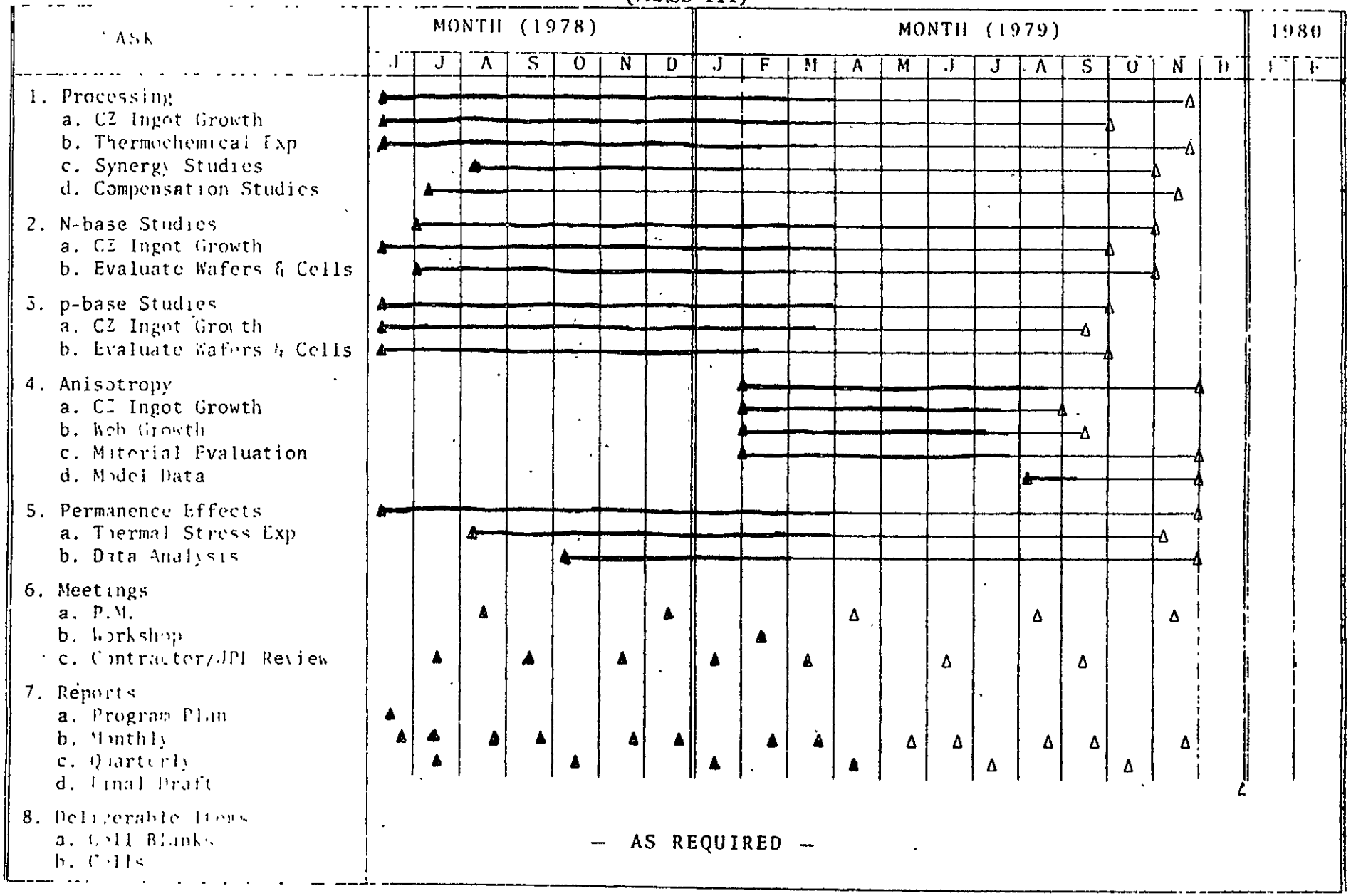

6. REFERENCES

1. R. H. Hopkins, et al., 11th Quarterly Report and Summary, Silicon Materials Task (Part 2) DOE/JPL 954331-78/3, July 1978.
2. R. H. Hopkins, et al., 5th Quarterly Report and Summary, Silicon Materials Task (Part 2) DOE/JPL 954331-77/1, January 1977.
3. R. H. Hopkins, et al., 3rd Quarterly Report, Silicon Materials Task (Part 2) DOE/JPL 954331-76/3, July 1976.
4. R. H. Hopkins, et al., 13th Quarterly Report, Silicon Materials Task (Part 2), DOE/JPL-954331-79/1, January 1979.
5. R. H. Hopkins, et al., 12th Quarterly Report, Silicon Materials Task (Part 2), DOE/JPL-954331-78/4, October 1978.
6. R. H. Hopkins, et al, 10th Quarterly Report, Silicon Materials Task (Part 2), DOE/JPL-954331-78/2, April 1978.
7. M. G. Yang, K. M. Koliwad and G. E. McGuire, J. Electrochem Soc. p. 675, 1975.
8. R. B. Campbell, et al., Array Automated Assembly Task DOE/JPL-954873-79/1, January 1979.

7. APPENDICES

7.1 Ingot Impurity Concentrations

7.2 Resistivity and Etch Pit Density of Phase III Ingots

7.3 Carbon and Oxygen Analysis of Phase III Ingots

PPENDIX 7.1

Ingot Impurity Concentration

Ingot Identification	Target Concentration $X10^{15}$ atoms/cm^3	Calculated Concentration $X10^{15}$ atoms/cm^3	Mass Spec. Analysis $X10^{15}$ atoms/cm
W-129-00-000 (7.6 cm.)	NA	NA	NA
W-130-00-000 (7.6 cm.)	NA	NA	NA
W-131-Mn-008 (7.6 cm.)	0.6	0.55	0.55
W-132-Ta-003	0.0002	0.0009	<0.5
W-133-00-000	NA	NA	NA
W-134-Ti-009	0.05	0.03	<0.25
W-135-Fe-005	1.0	0.78	<1.5
W-136-Fe-006	0.3	0.24	<1.5
W-137-Ti-010	0.21	0.21	<0.25
W-138-Mo-005	0.001	0.0008	<0.5
W-139-Mo-006	0.0042	0.0054	<0.5
W-140-Ti-011 (7.6 cm.)	0.18	0.18	<0.25
W-141-Mo/Cu-001	0.004/4.42	0.003/3.68	<0.5/4.00
W*-142-00-000	NA	NA	NA
W*-143-Ti-002	0.20	0.17	<0.25
W*-144-Mo-001	0.0042	0.0044	<0.5
W-145-W-001	Max. Conc.	Processing	Processing
W-146-Co-001	0.55	0.39	0.55
W-147-N/Ni-002	0.4	0.33	<1.5
W-148-N/Mn-002	0.60	0.76	0.55
W-149-N/Fe-003	0.60	0.58	<1.5
W-150-N/V-003	0.03	0.03	<0.15
W**-151-00-000	NA	NA	NA
W**-152-Ti-001	0.2	0.22	<0.25
W-153-N/Ti-003	0.01	0.017	<0.25
W-154-N/Cr-003	0.55	0.71	0.35
W-155-N/Mo-001	0.001	0.001	<0.50
W-156-N/Mo-002	0.004	0.003	<0.50

APPENDIX 7.1

Ingot Impurity Concentration (cont.)

Ingot Identification	Target Concentration $X10^{15}$ atoms/cm^3	Calculated Concentration $X10^{15}$ atoms/cm^3	Mass Spec. Analysis $X10^{15}$ atoms/cm^3
W-157-N/Ti/V-001	Ti: 0.10	0.08	<0.25
	V: 0.10	0.12	<0.15
W-158-N/Ti/V/Cr-001	Ti: 0.05	0.05	<0.25
	V: 0.05	0.05	<0.15
	Cr: 0.60	0.55	0.33
W-159-N/Cr/Mn/Ti/V-001	Cr: 0.4	0.35	0.20
	Mn: 0.4	0.32	0.25
	Ti: 0.02	0.02	<0.25
	V: 0.02	0.02	<0.15
W*-160-Ti-001	0.2	0.17	<0.25
W**-161-Ti-002	0.02	0.03	<0.25
W-162-Ni/Ti-001	Ni: 1.0	Processing	<1.5
	Ti: 0.2		<0.25
W-163-Ni/V-001	Ni: 1.0	Processing	<1.5
	V: 0.4		0.15
W-164-Ni/Mo-001	Ni: 1.0	Processing	<1.5
	Mo: 0.004		<0.5
W-165-Co-002	Co: 0.11	Processing	<0.55
W-166-Fe-007	Fe: 0.9	Processing	<1.5
W-167-Nb-001	Nb: Max	Processing	<0.15
W*-168-Ph-002	35	NA	(110)+
W*-169-Ph-004	47	NA	(136)+
W-170-Ph-005	66	NA	Processing
W-171-W-002	Max. Conc.	Processing	Processing

* Low resistivity p-type ingot ($\leq$ 1Ω-cm).

** 30 Ω-cm p-type ingot.

\+ Value based on resistivity measurement.

APPENDIX 7.2

Resistivity and Etch Pit Density of Phase III Ingots

Ingot Identification	TGT Resistivity (ohm-cm)	Actual Resistivity (ohm-cm)	Etch$^+$ Pit Density (/cm^2)
W-129-00-000 (7.6 cm)	4.0 (B)	4.7-3.0	1 K-Gross Lineage
W-130-00-000 (7.6 cm)	4.0 (B)	4.7-3.7	OK-Gross Lineage
W-131-Mn-008 (7.6 cm)	4.0 (B)	6.0-3.8	OK-Gross Lineage
W-132-Ta-003	4.0 (B)	3.8-3.4	1-20K
W-133-00-000	4.0 (B)	4.3-3.7	OK-Gross Lineage
W-134-Ti-009	4.0 (B)	4.9-4.4	0-10K
W-135-Fe-005	4.0 (B)	5.3-2.1	0-Gross Lineage
W-136-Fe-006	4.0 (B)	3.3-2.7	1K-Gross Lineage
W-137-Ti-010	4.0 (B)	4.6-4.4	0-Gross Lineage
W-138-Mo-005	4.0 (B)	5.0-4.1	0-5K
W-139-Mo-006	4.0 (B)	4.0-2.3	0-Gross Lineage
W-140-Ti-011 (7.6 cm)	4.0 (B)	3.6-1.7	5K-Gross Lineage
W-141-Mo/Cu-001	4.0 (B)	4.7-3.0	2K-Gross Lineage
W*-142-00-000	0.2 (B)	0.22-0.20	0-3K
W*-143-Ti-002	0.2 (B)	0.21-0.15	0-Gross Poly
W*-144-Mo-001	0.2 (B)	0.23-0.19	0-Gross Poly
W-145-W-001	4 (B)	4.5-4.0	2K-Gross Poly
W-146-Co-001	4 (B)	4.7-4.2	1K-Gross Poly
W-147-N/Ni-002	1.5 (P)	1.9-1.4	2-15K
W-148-N/Mn-002	1.5 (P)	2.5-2.1	1K-Gross Poly
W-149-N/Fe-003	1.5 (P)	2.0-1.6	3K-Gross Poly
W-150-N/V-003	1.5 (P)	2.0-1.5	1-5K
W**-151-00-000	30 (B)	35.6-18.1	0-5K
W**-152-Ti-001	30 (B)	31.9-25	0-Gross Poly
W-153-N/Ti-003	1.5 (P)	2.1-1.1	0-10K
W-154-N/Cr-003	1.5 (P)	2.1-1.4	3K-10K
W-155-N/Mo-001	1.5 (P)	1.9-1.8	1-4K
W-156-N/Mo-002	1.5 (P)	1.7-1.3	3K-Gross Poly
W-157-N/Ti/V-001	1.5 (P)	2.0-1.6	1-10K
W-158-N/Ti/V/Cr-001	1.5 (P)	2.1-1.6	1K-gross Lineage
W-159-N/Cr/Mn/Ti/V-001	1.5 (P)	2.0-1.8	1-2K

APPENDIX 7.2

Resistivity and Etch Pit Density of Phase III Ingots (Continued)

Ingot Identification	TGT Resistivity (ohm-cm)	Actual Resistivity (ohm-cm)	Etch+ Pit Density (/cm^2)
W*-160-Ti-001	1.0 (B)	1.3-1.0	2-8K
W**-161-Ti-002	30 (B)	31.8-21.7	1-15K
W-162-Ni/Ti-001	4.0 (B)	4.5-4.0	OK-Clusters
W-163-Ni/V-001	4.0 (B)	4.8-4.4	1K-Clusters
W-164-Ni/Mo-001	4.0 (B)	4.7-3.2	OK-Clusters
W-165-Co-002	4.0 (B)	4.5-3.8	0-5K
W-166-Fe-007	4.0 (B)	4.7-3.0	OK-Gross Lineage
W-167-Nb-001	4.0 (B)	4.0-5.7	OK-Poly
W*-168-Ph-002	0.5 (B)	0.41-0.50	3-10K
W*-169-Ph-004	1.0 (B)	Processing	Processing
W-170-Ph-005	2.9 (B)	Processing	Processing
W-171-W-002	4.0 (B)	Processing	Processing

* Low resistivity p-type ingot ($\leq$ 1 Ω-cm)

** Use of double asterisk indicates 30 ohm-cm p-type ingot

\+ The first figure is etch pit density of the seed; second figure etch pit density of extreme tang end of ingot. The first value shown is indicative of dislocation density in slices used for cell fabrication. Structural degredation commonly occurs at the tang end of the most heavily-doped ingots due to constitutional supercooling. (1)

APPENDIX 7.3

Carbon and Oxygen Concentrations

of Phase III Ingots

Ingot Number	Carbon Concentration x 10^{16} atoms/cm^3	Oxygen Concentration x 10^{16} atoms/cm^3
W-129-00-000	11.3	202
W-131-Mn-008	5.3	164
W-133-00-000	10.4	117
W-135-Fe-005	9.4	118
W-137-Ti-010	5.3	134
W-139-Mo-006	6.5	149
W-141-Mo/Cu-001	8.3	156
W*143-Ti-002	++	++
W-145-W-001	5.8	149
W-147-N/Ni-002	14.0	157
W-149-N/Fe-003	6.6	151
W**151-00-000 (30Ω-cm)	7.0	154
W-153-N/Ti-001	7.5	160
W-155-N/Mo-001	9.2	183
W-157-N/Ti/V-001	5.7	103
W-159-N/Cr-Mn/Ti/V-001	8.7	183
W**-161-Ti-002	6.0	138
W-163-Ni/V-001	5.0	128
W-165-Co-002	11.2	106
W-167-Nb-001	6.0	130
W*-169-Ph-004	++	++
W-171-W-002	Processing	Processing

* low resistivity ingot

** high resistivity ingot

++ Due to free carrier absorption infrared methods cannot be used for carbon and oxygen determination in these samples.

Low-Cost Solar Array Project

Contractor Quarterly, Annual, Interim, and Final Report Distribution List

Distribution List #644 - Silicon Material Task

	No. of copies
Adolph Meller Co. Attn: R. R. Monchamp P. O. Box 6001 Providence, RI 02940	1
Aerochem Research Laboratories Attn: Dr. H. F. Calcote P. O. Box 12 Princeton, NJ 08540	1
Aerospace Corporation Attn: H. J. Killan P. O. Box 92957 Los Angeles, CA 90009	1
Aerospace Corporation Attn: Dr. Stanley L. Leonard P. O. Box 92957 Los Angeles, CA 90009	1
Aerospace Corpration Attn: Mr. Howard Weiner Building A2 M/S 2037 P. O. Box 92957 Los Angeles, CA 9009	1
Alcoa Attn: Mr. Gregory Barthold 1200 Ring Bldg. Washington, DC 20036	1
Arco Solar, Inc. Attn: J. W. Yerkes 20554 Plummer Street Chatsworth, CA 91311	1
Argonne National Laboratory Attn: Dr. Steven Danyluk 9700 South Cass Avenue Argonne, IL 60439	1
Arizona State University College of Engr. Science Attn: Dr. Charles E. Backus Tempe, AZ 85281	1
Arthur D. Little, Inc. Attn: Dr. David Almgren Room 20-539 Acorn Park Cambridge, MA 02140	1
Dr. D. L. Bailey 627 West Ninth Street Traverse City, MI 49684	1
Battelle Memorial Institute Columbus Laboratory Attn: Mr. Melvin F. Browning 505 King Ave. Columbus, OH 43201	1
Battelle Memorial Institute Columbus Laboratory Attn: Dr. Donald C. Carmichael 505 King Ave. Columbus, OH 43201	1
The BDM Corporation Attn: Mr. J. Scott Hauger 7915 Jones Branch Drive McLean, VA 22101	1
Bernd Ross Associates Attn: Dr. Bernd Ross 2154 Blackmore Court San Diego, CA 92109	1
The Boeing Company Attn: Elizabeth Zimmerman M/S 88-05 P. O. Box 3999 Seattle, WA 98124	1
Boston College Department of Physics Attn: Professor Pao-Hsien Fang Chestnut Hill, MA 02167	1
Brown University Dept. of Engineering Attn: Dr. Joseph J. Loferski Providence, RI 02912	1

	No. of copies
C. T. Sah Associates Attn: Dr. C. T. Sah 403 Pond Ridge Lane Urbana, IL 61801	1
Calspan Corporation D-89 Attn: Dr. Charles W. Sauer P. O. Box 235 Buffalo, NY 14221	1
Carnegie-Mellon University Dept. Electrical Engineering Attn: Dr. Art Milnes Schenley Park Pittsburgh, PA 15213	1
City of Los Angeles Department of Water & Power Attn: Frank Goodman Room 1149 111 North Hope Street Los Angeles, CA 90051	1
Clarkson College of Technology Dept. of Chemical Engineering Attn: W. R. Wilcox Potsdam, NY 13676	1
Clemson University Dept. of Elect. & Computer Engr. Attn: Dr. John L. Prince Riggs Hall Clemson, SC 29631	1
Commander U. S. Army/MERADCOM Attn: DRDME-E/Mr. Donald D. Faehn Fort Belvoir, VA 22060	1
Comsat Laboratories Attn: Dr. Denis Curtin 22300 Comsat Drive Clarksburg, MD 20734	1
Coors Porcelain Company Attn: Mr. David Wirth 600 Ninth Street Golden, CO 80401	1
Corning Glass Works Industrial Products Development Attn: Mr. Raymond Ambrogi Corning, NY 14830	1
Crystal Systems, Inc. Attn: Frederick Schmid Shetland Industrial Park P. O. Box 1057 Salem, MA 01970	1
Deposits & Composites Inc. Attn: Richard E. Engdahl 318 Victory Drive Herndon, VA 22070	1
Dow Corning Corporation Solid State Research Attn: Dr. L. D. Crossman 12534 Geddes Road Hemlock, MI 48626	1
Dow Corning Corporation Attn: C. G. Currin Midland, MI 48640	1
Eagle Picher Industries, Inc. Attn: Mr. Paul Grayson P. O. Box 1076 Miami, OK 74354	1
Electric Power Research Institute Attn: E. A. DeMeo 3412 Hillview Avenue P. O. Box 10412 Palo Alto, CA 94304	1
Electro Oxide Corporation Attn: Frank St. John P.O. Box 15376 West Palm Beach, FL 33406	1
Energy Materials Corporation Attn: Dave Jewett 30 Faulkner Street Ayer, MA 01432	1
Exotic Materials Inc. Attn: W. L. Loucks 2988 Randolph Avenue Costa Mesa, CA 92626	1

	No. of copies
Exxon Research & Engineering Co. Attn: Dr. James Amick P. O. Box 8 Linden, NJ 07036	1
General Electric Company Valley Forge Space Center Attn: Aaron Kirpich P. O. Box 8555 Philadelphia, PA 19101	1
General Electric Company Corporate Research & Development Attn: M. Garfinkel P. O. Box 43 Schenectady, NY 12301	1
General Electric Company Valley Forge Space Center Attn: G. J. Rayl Room M2445 P. O. Box 8555 Philadelphia, PA 19101	
Grumman Energy Systems, Inc. Advanced Concepts Attn: Mr. Edward Diamond 4175 Veterans Memorial Highway Ronkonkoma, NY 11779	1
Honeywell, Inc. Corporate Technology Center Attn: J. D. Heaps 10701 Lyndale Avenue South Bloomington, MN 55420	1
IBM Corporation Attn: Dr. G.H. Schwuttke East Fishkill, Rt. 52 Hopewell Junction, NY 12533	1
IBM Federal Systems Division Attn: Donald F. Erat 18100 Frederick Pike Gaithersburg, MD 20760	1
ICT, Inc. Attn: L. P. Kelley 1330 Industrial Drive Shelby, MI 49455	1
International Rectifier Semiconductor Division Attn: M. F. Gift 233 Kansas Street El Segundo, CA 90245	1
J. C. Schumacher Company Attn: John C. Schumacher 580 Airport Road Oceanside, CA 92054	1
Jet Propulsion Laboratory Attn:(Contract Negotiator) M/S 506-401 4800 Oak Grove Drive Pasadena, CA 91103	1
Jet Propulsion Laboratory LSA Project Data Center Attn: Mrs. Loretta Steward M/S 506-451 4800 Oak Grove Drive Pasadena, CA 91103	50
Jet Propulsion Laboratory Technical Information Division Attn: G. A. Mitchell, 111-141 4800 Oak Grove Drive Pasadena, CA 91103	4 + Repr
Jet Propulsion Laboratory Technology Utilization Attn: L. P. Speck M/S 180-302 4800 Oak Grove Drive Pasadena, CA 91103	1
Kayex Corporation Hamco Division Attn: R. L. Lane 1000 Millstead Way Rochester, NY 14624	1
Lamar University Attn: Dr. Keith Hansen P. O. Box 10022 Beaumont, TX 77710	1

No. of copies

Lamar University
Attn: Dr. Ku-Yen Li
P. O. Box 10053
Beaumont, TX 77710 — 1

Lamar University
Attn: Dr. Wayne Sanders
P. O. Box 10028
Beaumont, TX 77710 — 1

Lamar University
Attn: Dr. Carl L. Yaws
P. O. Box 10053
Beaumont, TX 77710 — 1

Lockheed Missiles & Space Co.
Attn: L. G. Chidister
Dept. 62-25, Bldg. 151
P. O. Box 504
Sunnyvale, CA 94088 — 1

Lockheed Missiles & Space Co.
Attn: Paul Dillard
Dept. 62-25, Bldg. 151
P. O. Box 504
Sunnyvale, CA 94088 — 1

Los Alamos Scientific Laboratory
Attn: S. W. Moore
Group Q-11, Mail Stop 571
Los Alamos, NM 87545 — 1

Massachusetts Institute of Tech.
Lincoln Laboratory
Attn: Mr. Ron Matlin
Room I-210
P. O. Box 73
Lexington, MA 02173 — 1

Massachusetts Institute of Tech.
Lincoln Laboratory
Attn: Mr. Marvin Pope
Room I-210
P. O. Box 73
Lexington, MA 02173 — 1

Massachusetts Institute of Tech.
Attn: Dr. Richard Tabors
Building E-38, Room 400
Cambridge, MA 02139 — 1

Dr. H. F. Matare
P. O. Box 49177
Los Angeles, CA 90049 — 1

Materials Research, Inc.
Attn: Dr. Ram Natesh
700 South 790 East
Centerville, UT 84014 — 1

MB Associates
Attn: Mr. Len Foote
Bollinger Canyon Road
San Ramon, CA 94583 — 1

MB Associates
Attn: Mr. Robert Mainhardt
Bollinger Canyon Road
San Ramon, CA 94583 — 1

McDonnell Douglas Astronautics Co-East
Materials & Processes
Attn: Mr. L. G. Harmon
Bldg. 106/4/E7
St. Louis, MO 63166 — 1

McGraw-Edison Company
Edison Battery Division
Attn: D. P. Spittlehouse
210 Redstone Hill Road
Bristol, CT 06010 — 1

Mobil Tyco Solar Energy Corp.
Attn: A. I. Mlavsky
16 Hickory Drive
Waltham, MA 02154 — 1

Mobil Tyco Solar Energy Corp.
Attn: K. V. Ravi
16 Hickory Drive
Waltham, MA 02154 — 1

Monsanto Research Corporation
Attn: H. Gutsche
P. O. Box 8
St. Peters, MO 63376 — 1

	No. of copies
Motorola, Inc. Semiconductor Group Attn: R. Gurtler 5005 East McDowell Road Phoenix, AZ 85008	1
Motorola, Inc. Semiconductor Group Attn: William Ingle, B136 5005 East McDowell Road Phoenix, AZ 85008	1
Motorola, Inc. Semiconductor Group Attn: I. Arnold Lesk 5005 East McDowell Road Phoenix, AZ 85008	1
Motorola, Inc. Semiconductor Group Attn: R. McGinnis 5005 East McDowell Road Phoenix, AZ 85008	1
Motorola, Inc. Semiconductor Group Attn: D. Rosler 5005 East McDowell Road Phoenix, AZ 85008	1
Mount Edison USA, Inc. Attn: Marrith Kasters 1114 Avenue of the Americas New York City, NY 10036	1
NASA Headquarters Office of Energy Programs Attn: John Loria Code RET-14 Washington, DC 20546	1
NASA Headquarters Attn: J. P. Mullin Code RP-5, M/S B636 Washington, DC 20546	1
NASA Lewis Research Center Photovoltaic Project Office Attn: Roger S. Palmer M/S 49-5 21000 Brookpark Road Cleveland, OH 44135	5
National Bureau of Standards Attn: Dr. Sam Coriell Transformation & Kinetics Sect. Metallurgy Division Washington, DC 20234	1
National Science Foundation Division of Applied Research Attn: Dr. Tapan Mukherjee 1800 G. Street N.W. Washington, DC 20550	2
Naval Underwater Systems Center Attn: Dr. R. Santopietro Code 313 Building 28 New London, CT 06320	1
Nav-Tec Industries Attn: Mr. Norman Sandys 87 Bethpage Road Hicksville, NY 11802	1
Northeast Solar Energy Center Attn: Dr. Solomon Zwerdling 70 Memorial Drive Cambridge, MA 02142	1
Northeastern University Mechanical Eng. Branch/Campus Attn: W. B. Nowak 360 Huntington Avenue Boston, MA 02115	1
Optical Coating Laboratory, Inc. Attn: D. Sharman 15251 East Don Julian Road City of Industry, CA 91746	1
Opto Technology, Inc. Attn: W. E. Hegberg 1674 South Wolf Road Wheeling, IL 60090	1
Owens Illinois, Inc. Attn: G. L. Glen P. O. Box 1035 Toledo, OH 43666	1

	No. of copies
The Perkin-Elmer Corporation Electro-Optical Division Attn: Dr. Burke E. Nelson Norwalk, CT 06856	1
PRC Energy Analysis Company Attn: Mr. Arie P. Ariotedjo 7600 Old Springhouse Road McLean, VA 22101	1
RCA Laboratories David Sarnoff Research Center Attn: G. W. Cullen Box 800 Princeton, NJ 08540	1
RCA Laboratories David Sarnoff Research Center Attn: Dr. David Richman Princeton, NJ 08540	1
RCA Laboratories David Sarnoff Research Center Attn: Dr. Arthur Sherman P. O. Box 432 Princeton, NJ 08540	1
RCA Laboratories David Sarnoff Research Center Attn: B. F. Williams Princeton, NJ 08540	1
Rockville Refining Company Attn: Bernard Free Unit 3 7800 Airpark Road Gaithersburg, MD 20760	1
Rockwell International Corp. Electronics Research Center Attn: Dr. R. P. Ruth D/540, HA32 3370 Miraloma Avenue Anaheim, CA 92803	2
Sandia Laboratories Division 4719 Attn: Dr. Donald G. Schueler Albuquerque, NM 87185	1
Science Applications, Inc. Attn: Dr. J. A. Naber P. O. Box 2351 1200 Prospect Street La Jolla, CA 92037	1
Semiconductor Processing Company Attn: Mr. Mayburg 10 Industrial Park Road Hingham, MA 02043	1
Sensor Technology, Inc Attn: I. Rubin 21012 Lassen Street Chatsworth, CA 91311	1
Shell Development Company Attn: Karl T. Geoca P. O. Box 2463 Houston, TX 77001	1
Siltec Corporation Attn: R. E. Lorenzini 3717 Haven Avenue Menlo Park, CA 94025	1
Sol/Los, Inc. Attn: Milo Macha 2231 South Carmelina Avenue Los Angeles, CA 90064	1
Solamat, Inc. Attn: Dr. Barton Roessler 4 Indigo Road Barrington, RI 02806	1
Solar Energy Research Institute Attn: Dr. Charles J. Bishop 1536 Cole Blvd. Golden, CO 80401	1
Solar Energy Research Institute Attn: Wendy Jackson 1536 Cole Blvd. Golden, CO 80401	1
Solar Energy Research Institute Attn: Dr. Paul Rappaport 1536 Cole Blvd. Golden, CO 80401	1
Solar Energy Research Institute Attn: Dr. Matthew Sandor 1536 Cole Blvd. [illegible]	1

	No. of copies
Solar Energy Research Institute Photovoltaic Branch Attn: Ted Cizek 1536 Cole Blvd. Golden, CO 80401	1
Solar Energy Research Institute Photovoltaic Program Office Attn: Dr. Tom Surek 1536 Cole Boulevard Golden, CO 80401	1
Solar Energy Research Institute Photovoltaic Program Office Attn: Dr. C. Edwin Witt 1536 Cole Blvd. Golden, CO 80401	1
Solar Power Corporation Attn: P. Caruso 5 Executive Park Drive North Billerica, MA 01862	1
Solarex Corporation Attn: John V. Goldsmith 1335 Piccard Drive Rockville, MD 20850	1
Solarex Corporation Attn: Dr. Joseph Lindmayer 1335 Piccard Drive Rockville, MD 20850	1
Solec International, Inc. Attn: Ishaq Shahryar Suite 484 Two Century Plaza 2049 Century Park East Los Angeles, CA 90067	1
Southern Methodist University Institute of Technology Electrical Engineering Dept. Attn: T. L. Chu Dallas, TX 75275	1
Spectrolab, Inc. Attn: E. L. Ralph 12500 Gladstone Avenue Sylmar, CA 91342	1
Spectrolab, Inc. Attn: W. Taylor 12500 Gladstone Avenue Sylmar, CA 91342	1
Spire Corporation Patriots Park Attn: Allen R. Kirkpatrick P. O. Box D Bedford, MA 01730	1
Stanford Research Institute Attn: Vijay Kapur Menlo Park, CA 94025	1
Stanford Research Institute Attn: Dr. Leonard Nanis Menlo Park, CA 94025	1
Stanford University Center for Materials Research Attn: Dr. Robert S. Fiegelson Stanford, CA 94305	1
Stanford University Stanford Electronics Labs Attn: J. F. Gibbons Stanford, CA 94305	1
Stanford University Solid State Electronics Lab Attn: Professor G. Pearson Stanford, CA 94305	1
State University of New York College of Engineering Department of Materials Science Attn: Dr. Franklin F. Y. Wang Stony Brook, NY 11794	1
Synthatron Corporation Attn: Hilliard Blanck 50 Intervale Rd. Parsippany, NJ 07054	1
Technion Incorporated Attn: G. L. Cann Suite F 11751 Sky Park East Irvine, CA 92707	1

	No. of copies
Texas Instruments, Inc. Attn: Dr. John Robinson Mail Stop 850 Highway 75 Sherman, TX 75090	1
Texas Instruments, Inc. Semiconductor Group Attn: S. N. Rea, M/S 960 P. O. Box 225012 Dallas, TX 75222	1
Texas Instruments, Inc. Semiconductor Group Attn: Dr. Gene Wakefield Mail Stop 82 P. O. Box 225012 Dallas, TX 75222	1
TRW Systems Group Attn: Paul Goldsmith Bldg. M1/1334 One Space Park Redondo Beach, CA 90278	1
Union Carbide Corporation Chemical and Plastics Attn: W. Breneman P. O. Box 180 Sistersville, WV 26175	1
Union Carbide Corporation Chemicals & Plastics Attn: Dr. P. J. Orenski Silicones Building Tarrytown, NY 10591	1
Union Carbide Corporation Linde Division Attn: Dr. Hiroshi Morihara P. O. Box 44 Tonawanda, NY 14150	1
Union Carbide Corporation Tarrytown Technical Center Attn: Dr. Pesho Kotval Corporate Research Building Tarrytown, NY 10591	1
Union Carbide Corporation Technical Information Service P. O. Box 6116 Cleveland, OH 44101	1
United Detector Technology, Inc Attn: P. Wendland 2644-30th Street Santa Monica, CA 90405	1
University of Delaware College of Engineering Attn: Professor Karl W. Boer Du Pont Hall Newark, DE 19711	1
University of Missouri-Rolla Ceramic Engineering Department Attn: Dr. P. Darrell Ownby Rolla, MO 65401	1
University of New Mexico Bureau of Engineering Research Faris Engineering Center Attn: W. W. Grannemann, Room 124 Albuquerque, NM 87131	1
University of Pennsylvania Attn: Professor Martin Wolf 308 Moore D2 Philadelphia, PA 19174	1
University of South Carolina College of Engineering Attn: R. B. Hilborn, Jr. Columbia, SC 29208	1
U. S. Department of Energy Division of Solar Technology Attn: Dr. Leonard M. Magid 600 E. Street, N. W. Washington, DC 20545	1

	No. of copies
U. S. Department of Energy Division of Solar Technology Attn: Mr. P. D. Maycock 600 E. Street, N.W. Washington, DC 20545	1
U. S. Department of Energy Division of Solar Technology Attn: Dr. Morton Prince 600 E. Street, N.W. Washington, DC 20545	1
U. S. Department of Energy Technical Information Center Attn: T. B. Abernathy P. O. Box 62 Oak Ridge, TN 37830	2 + Repro
Varian Associates Lexington Vacuum Division Attn: Dr. John A. Decker, Jr. 121 Hartwell Avenue Lexington, MA 02173	1
Virginia Semiconductor, Inc. Attn: Dr. Thomas G. Digges, Jr. 1000 Jefferson Davis Highway Fredericksburg, VA 22401	1
Westech Systems, Inc. Attn: G. L. Gill, Jr. 4225 South 37th Street Phoenix, AZ 85040	1
Western Electric Semiconductor Materials Engineering Attn: R. E. Ruesser - 3510 555 Union Blvd. Allentown, PA 1893	1
Westinghouse Electric Corporation Power Circuit Breaker Div. ARC Heater Project Attn: Dr. M. Fey Trafford, PA 15085	1
Westinghouse Electric Corporation Research Laboratories Attn: J. R. Davis M/S 501/2D28 1310 Beulah Road Pittsburgh, PA 15235	1
Westinghouse Electric Corporation Research Laboratories Attn: R. H. Hopkins 1310 Beulah Road Pittsburgh, PA 15235	1
Westinghouse Electric Corporation Research Laboratories Attn: Dr. R. Mazelsky 1310 Beulah Road Pittsburgh, PA 15235	1
Westinghouse Electric Corporation Research Laboratories Attn: Dr. P. F. Pittman 1310 Beulah Road Pittsburgh, PA 15235	1
Westinghouse Electric Corporation Research Laboratories Attn: Dr. P. Rai-Choudhury 1310 Beulah Road Pittsburgh, PA 15235	1
Westinghouse Electric Corp. Research Laboratories Attn: R. K. Riel 1310 Beulah Road Pittsburgh, PA 15235	1
Xerox Electro-Optical Systems Attn: Mr. Keith Winsor 300 North Halstead Pasadena, CA 91107	1